2020

Synthesis of Au-Ag Alloy Nanoparticles and Characterization of Nanoparticle-Anthracene Hybrid Materials

XIANG ZHOU
University of Pennsylvania, caesardarcy@gmail.com

Synthesis of Au-Ag Alloy Nanoparticles and Characterization of Nanoparticle-Anthracene Hybrid Materials

Abstract

In this work, the optical properties of Au-Ag alloys with an anthracene ligand grafter to their surfaces was examined. Structurally and chemically homogeneous Au-Ag alloy NPs were synthesized by a seed-mediated method with the Ag precursor reduced and grown onto the prepared Au seeds. The alloy NPs were formed after inter-diffusion of Au and Ag and protected using oleylamine. Functionalization of the metal NPs with the anthracene-incorporated ligands was conducted via a simple ligand exchange protocol. The morphological information and chemical composition of the resulting NPs were confirmed by transmission electron microscopy and energy dispersive X-ray spectroscopy, respectively. The plasmonic effect of the metal NPs on the fluorescence was examined using Ultraviolet-visible and fluorescence spectroscopy. The plasmonic enhancement of the fluorescence was found to be varied among different compositions of the alloy NPs.

Keywords

gold-silver alloy nanoparticles, plasmon resonance, surface-enhanced fluorescence

Disciplines

Chemistry | Materials Chemistry

AN ABSTRACT OF THE CAPSTONE REPORT OF

Xiang Zhou for the Degree of Master of Chemical Sciences

Title: *Synthesis of Au-Ag Alloy Nanoparticles and Characterization of Nanoparticle-Anthracene Hybrid Materials*

Project conducted at: Department of Chemistry
University of Pennsylvania
231 S. 34th Street, Philadelphia, PA 19104-6323
Supervisor: Christopher B. Murray
Dates of Project: Feb 1, 2019 – May 18, 2020

Abstract Approved:

Christopher B. Murray, Principle Investigator

In this work, the optical properties of Au-Ag alloys with an anthracene ligand grafter to their surfaces was examined. Structurally and chemically homogeneous Au-Ag alloy NPs were synthesized by a seed-mediated method with the Ag precursor reduced and grown onto the prepared Au seeds. The alloy NPs were formed after inter-diffusion of Au and Ag and protected using oleylamine. Functionalization of the metal NPs with the anthracene-incorporated ligands was conducted via a simple ligand exchange protocol. The morphological information and chemical composition of the resulting NPs were confirmed by transmission electron microscopy and energy dispersive X-ray spectroscopy, respectively. The plasmonic effect of the metal NPs on the fluorescence was examined using Ultraviolet-visible and fluorescence spectroscopy. The plasmonic enhancement of the fluorescence was found to be varied among different compositions of the alloy NPs.

Synthesis of Au-Ag Alloy Nanoparticles and Characterization of Nanoparticle-Anthracene Hybrid Materials

by

Xiang Zhou

A CAPSTONE REPORT

submitted to the

University of Pennsylvania

in partial fulfillment of
the requirements for
the degree of

Master of Chemical Sciences

Presented on April 22, 2020

Commencement on May 18, 2020

Master of Chemical Sciences Capstone Report of Xiang Zhou Presented on April 22, 2020.

APPROVED:

Prof. Christopher B. Murray, Representing Materials Chemistry

I understand that my Capstone Report will become part of the permanent collection of the University of Pennsylvania Master of Chemical Sciences Program. My signature below authorizes the release of my final report to any reader upon request.

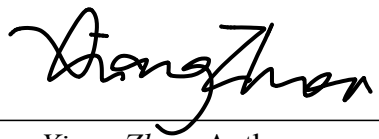

Xiang Zhou, Author

Acknowledgements

I would like to express my deep gratitude to Professor Christopher B. Murray, my research supervisor, for his patient direction, generous encouragement and valuable critiques of this project. I would like to thank Dr. Ana-Rita Mayol for her professional guidance and valuable support during my master's program. I would also like to thank Katherine Elbert, for her assistance and help in keeping my progress in schedule. My grateful thanks are also extended to Daniel Rosen, who trained me the use of X-ray diffractometer and who is always willing to give a helping hand, to Dr. Guillaume Gouget for his help in doing the EDS characterization and data analysis for me. I would also like to extend my thanks to all the members of the Murray lab for their support during the past whole year. Special thanks to my parents and Ching, for their encouragement and support throughout my life.

Table of Contents

List of Figures

List of Tables

List of Appendices

Introduction

Metal nanoparticles (NPs) are the subject of much research interest in recent decades due to their unique optical properties.[1-3] In particular, noble metals including copper, gold and silver NPs exhibit strong absorption of visible light in a broad region of the spectrum.[1] Interestingly, these colloidal metal NPs show brilliant colors, which are quite different from bulk materials composed of the same elements. This phenomenon, which is also denoted as surface plasmon resonance, can be explained by the collective oscillation of the free electrons in the conduction band of the metal induced by the incident light, which contributes to an enhancement in the local electromagnetic field.[1-4]

Plasmonics have wide applications and are intriguing for both chemical and biomedical use in imaging,[3,5] catalysis,[5,6] and sensing.[5,7,8] Research on plasmonic properties has been conducted based on pure Au and Ag NPs in great detail.[1-5] Moreover, the Au-Ag alloy systems are also being prevalently studied,[1,9-11] as the plasmonic properties can be easily tuned by changing the intrinsic properties of the NPs apart from the morphology of the NPs. The plasmon bands can also be altered by the alloy composition. Due to a linear relationship between the absorption maximum wavelength and the composition, the extinction peaks can be quantitatively adjusted within a relatively wide range from 380 to 520 nm, which are the featured plasmon resonance bands of Ag and Au, respectively.[10,11]

When bringing the plasmonic NPs in close vicinity to a fluorescent molecule, specific interactions between the metal surfaces and the adjacent fluorophores induced by incident light may lead to an enhanced or diminished radiation.[2,8,12] Many factors contribute to the plasmonic enhancement or the quenching of the radiative emission, including intrinsic parameters of the metal NPs that have been described above and the characteristics of the fluorescent molecules.[8,13] The separation between the metal surfaces and the fluorophores also plays an important part on the fluorescence efficiency.[12] Furthermore, a significant improvement in fluorescent efficiency was reported when there is a spectral overlap between the plasmon resonance band of the metal NPs and the absorption band of the dye compound.[12,14] Other environmental effects include but are not limited to the permittivity of the surrounding media.[11] In consideration of all the factors discussed above, it is of great importance to control variables when quantitatively studying the relationship between different compositions of the NPs and the corresponding plasmonic enhancement on the radiative emission of the fluorophore.

The goal of this work is to determine the relationship between the compositions of the Au-Ag alloy NPs and the resulting plasmonic effect on fluorescence of a dye molecule, anthracene. To achieve this, a series of monodisperse Au_xAg_{1-x} alloy NPs ($0 \leq x \leq 1$) with six different compositions and nearly identical sizes of 7.5 nm will be synthesized, and their corresponding plasmonic properties studied. They will be denoted as Ag, $AuAg_4$, Au_2Ag_3, Au_3Ag_2, Au_4Ag, and Au NPs based on the relative composition of each sample. Two dendrimer ligands were selected and synthesized within the Murray group (**Figure 1**). These two ligands exhibit similar steric bulkiness with hydrocarbon tails composed of 12 carbons. It was reported previously that this particular architecture of dendrimer ligands adds significant chemical and colloidal stability to metal NPs, which helps improve NP

lifetime.[6,14,15] Both ligands contain a disulfide group and are expected to possess similar binding affinity to the surface of the NPs. The only difference is that dendrimer **1** is incorporated with a fluorescent molecule, anthracene, while **2** serves as the control ligand. Anthracene, a molecule containing a conjugated aromatic system, can be excited and emits light in the visible region of the spectrum.[16] Additionally, anthracene shows extraordinary fluorescent properties and photostability that have been studied extensively.[17] Combination of the properties of dendrimer ligands and anthracene allows the organic molecules to exhibit high stability and fluorescence efficiency.

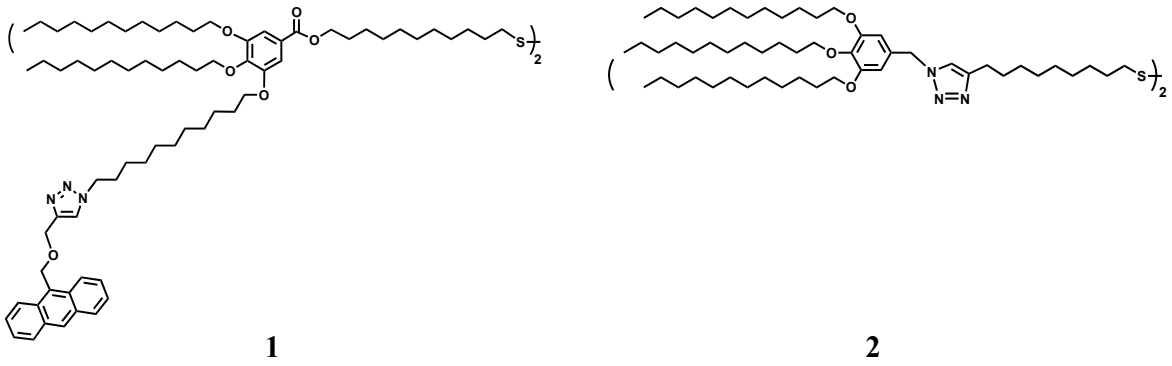

1 **2**

Figure 1. Molecular structure of dendrimer ligands **1** and **2**.

Generally, this work consists of three major stages: synthesis of Au-Ag alloy NPs, ligand exchange with anthracene-containing-dendrimers, and property assessment of the hybrid materials. In each stage, the persistency of composition, size distribution, and the shape of the NPs is confirmed using characterization techniques including EDS, XRD and UV-vis. The optical properties are assessed using UV-vis and fluorescence spectrophotometer.

Materials and Methods

Chemicals

n-Tetradecylphosphonic acid (TDPA) was purchased from PCI synthesis. $HAuCl_4 \cdot 3H_2O$ (≥ 99.9 % Au), $AgNO_3$ (99.9999 %), trioctylamine (98 %), oleylamine (Olam, 70 %), Olam (86 %), 1-octadecene (ODE, 90 %), 1-dodecanethiol (DDT, ≥ 98 %), 1,2,3,4-tetrahydronaphthalene (tetralin, 99 %), silver acetate (AgAc, ≥ 99 %) and borane tert-butylamine (TBAB, 97 %) were purchased from Sigma-Aldrich without further purification. Hexane, ethanol, isopropanol, chloroform and toluene were purchased from Fisher Scientific. All the solvents were ACS grade or higher and were used as received.

Synthesis of Au NPs (3 sizes: Au@Olam, 5 nm, 6 nm, and 7 nm)

The synthesis of Au NPs was conducted following reported procedures with slight modification.[6] To synthesize 5 nm Au NPs, 200 mg of $HAuCl_4 \cdot 3H_2O$ was dissolved in 10 mL of tetralin and 10 mL of Olam with sonication. The prepared Au precursor solution was then stirred under nitrogen and cooled in an ice bath for 30 minutes, followed by rapid injection of a solution of 90 mg of TBAB in 1 mL of tetralin and 1 mL of Olam. The color of the reaction solution gradually changed from orange to purplish red in minutes. The reaction was held in the ice bath for 3 hours before it was quenched using 120 mL of acetone. The Au NPs were isolated by centrifugation at a rate of 6000 rpm for 5 minutes, which were redispersed in hexane and purified twice using ethanol. The cleaned Au NPs were suspended in hexane for further use.

To synthesize 6 nm Au NPs, a modified seeded-growth method was used.[10] Specifically, a Au precursor solution was made by dissolving 85 mg of $HAuCl_4 \cdot 3H_2O$ in 10 mL of Olam and 10 mL of ODE, to which 5 mL of 10 mg/mL Au seeds in hexane was added. The reaction mixture was degassed at room temperature for 30 minutes and subsequently heated to 80 °C under a nitrogen atmosphere. After 2 hours of reaction, the resulting solution was quenched by addition of 40 mL of ethanol, followed by centrifugation at 6000 rpm for 3 minutes. The precipitated Au NPs were redispersed in hexane and protected by excess Olam ligands. The synthesis of 7 nm Au NPs followed the same synthesis procedure, except 5 mL of Olam and 5 mL of ODE were used based on 25 mg of Au seeds.

Synthesis of Ag NPs

Method 1

The Ag NP synthesis was performed using the Murray group's process,[10] where 278 mg of TDPA, 333 mg of AgAc and 20 mL of triotcylamine were mixed in a 50 mL round bottom-flask and stirred under nitrogen for 15 minutes. With vigorous stirring, the mixture was heated to 150 °C at a rate of ca. 15 °C/minute and held at 150 °C for another 20 minutes. After natural cooling to room temperature, the resulting blackish yellow product was purified using 40 mL of isopropanol, followed by centrifugation at 6000 rpm for 3 minutes. The precipitate was redispersed in hexane to give a yellow-brown suspension. The washing step was repeated three times to remove excess ligands. A few drops of Olam were added for longer preservation. Method 1 was used during summertime.

Method 2

Another way to synthesize monodisperse Ag NPs was based on a previously reported method.[19] Specifically, 170 mg of $AgNO_3$ and 20 mL of Olam (86 %) were loaded into a 50 mL round bottom-flask, which was sequentially heated to 60 °C under a nitrogen atmosphere until $AgNO_3$ precursor was completely dissolved. The reaction mixture was then heated to 140 °C and held for 3 hours before it was air cooled to room temperature. The purification of the product followed the above-mentioned washing procedure, except a total amount of 60 mL of acetone was used as the antisolvent. Method 2 was used in dry seasons.

Synthesis of AuAg alloy NPs

AuAg alloy NPs were synthesized using a reported method,[10] where Ag NPs were grown onto Au seeds.[2] A newly prepared 20 mg/mL Ag precursor solution was made by dissolving 120 mg of AgAc in 3mL of Olam and 3mL of ODE at 60 °C under a nitrogen atmosphere. A solution of 40 mg of Au seeds in 10 mL of OLAM and 10 mL of ODE were degassed at 80 °C for 30 minutes to ensure complete removal of oxygen and water. The seeds were then heated to 225 °C at a rate of 20 °C/minute. At 120 °C, a calculated amount (**Table 1**) of the fresh Ag precursor solution was injected to the Au solution drop by drop at a rate of 5 mL/hour. After completion of the injection, the reaction solution was held at 225 °C for another 20 minutes. To purify the product, the air-cooled NPs were isolated by acetone/ethanol precipitation and centrifugation. The alloy NPs were resuspended in hexane and washed twice more before they were stored in hexane with excess Olam ligands.

Table 1. Calculated amount of Au seeds and AgAc solution used to synthesize Au_xAg_{1-x}@Olam with four compositions.

Samples	Size of Au seeds (nm)	Quantities of Precursors	
		Dried Au seeds (mg)	AgAc solution (mL)*
$AuAg_4$	5	40	5.76
Au_2Ag_3	5	40	2.15
Au_3Ag_2	7	40	0.96
Au_4Ag	7	40	0.36

* 20 mg/mL AgAc solution was prepared by dissolving AgAc in a mixture of Olam and ODE (1:1).

Size Selection

To the NP solution**,** antisolvent (ethanol for Au NPs, isopropanol for Ag and Au-Ag alloy NPs) was added dropwise until the NP solution just started to become turbid. The suspension was centrifuged at a rate of 4000 rpm for 2 minutes and a flocculation fraction rich in large particles was collected as a pellet at the bottom of the centrifuge tube while smaller ones remained in the supernatant. The supernatant was carefully decanted, and hexane was added to redisperse the isolated NPs. Such procedure was repeated until the supernatant appeared clear.

Ligand Exchange with Thiol Ligands

All the ligand exchanges were performed following a previously reported procedure.[15] The ligand solution was prepared by dissolving 10 mg of thiol ligands in 2 mL of chloroform with vigorous magnetic stirring, to which a 10 mg/mL NP solution in hexane was added. All the ligand exchange reactions were carried out at room temperature for at least 1 h to achieve full exchange of the capping ligands. The NPs were flocculated by addition of ethanol, precipitated by centrifugation and collected in hexane or chloroform. This process was conducted five times to ensure complete removal of excess free ligands. The thiol-ligand capped NPs were stored in hexane or chloroform depending on the solubility of the NPs.

Characterization

Transmission electron microscopy (TEM) micrographs were imaged using a JEOL JEM-1400 microscope operated at 120 kV. High resolution TEM (HRTEM) images and EDS data were obtained using a JEOL JEM-1400 microscope. Plasmon cleaning and beam-shower technique were applied to remove carbon contamination before data acquisition. ^{1}H NMR (500 MHz) spectra were recorded on a Bruker UNI500 NMR. Chemical shifts were reported in parts per million (ppm) relative to deuterated chloroform ($CDCl_3$, 7.23 ppm). X-ray diffraction pattern of the NPs was acquired using a Rigaku D/MAX 2400 X-ray diffractometer at 40 kV. The XRD data were collected in the range of 2θ (degrees) varying from 30 ° to 90 ° using Cu-Kα radiation (λ = 1.541 Å). The UV-vis spectra were recorded at room temperature on a Cary 5000 UV–vis–NIR spectrometer using 1-cm quartz cuvettes. The fluorescence spectra were obtained using an Edinburgh fluorescence spectrometer.

Results and Discussion

Au_xAg_{1-x}@Olam samples with a specific dimension (7.5 nm) were synthesized to probe how the plasmon resonance bands effect the absorption or emission bands of the anthracene. The shape and size of the samples were tailored to be similar, to have a highly comparable sample set. Six Au_xAg_{1-x}@Olam samples were synthesized with their sizes targeted at around 7 nm. The average diameter size of all the metal NPs is 7.5 nm (7.00 to 8.12 nm) and the size distribution ranges from 4 % to 13 % (**Table 2**). The structural uniformity of the Au_xAg_{1-x}@Olam NPs was confirmed using TEM (**Figure 2**).

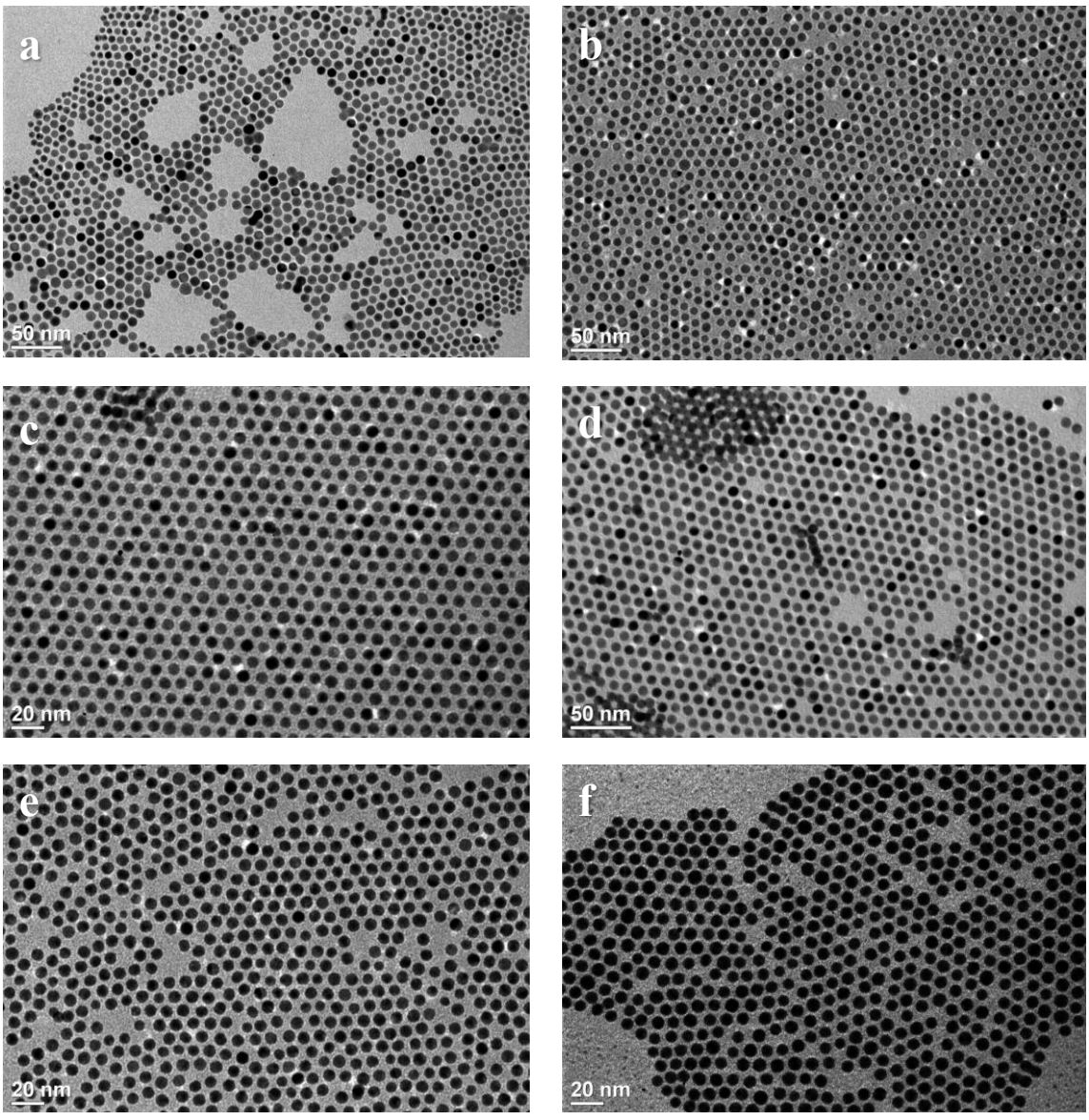

Figure 2. TEM images of Au_xAg_{1-x}@Olam NPs (a) $AuAg_4$ (8.09 ± 1.06 nm), (b) Au_2Ag_3 (8.12 ± 0.78 nm), (c) Au_3Ag_2 (7.04 ± 0.43 nm), (d) Au_4Ag (8.04 ± 0.46 nm), (e) Au (7.00 ± 0.46 nm), (f) Ag (7.27 ± 0.58 nm).

Table 2. The metal mole fraction measured by EDS, diameter sizes and maximum absorption wavelength of Au_xAg_{1-x}@Olam, Au@Olam and Ag@Olam NPs.

Samples	Metal Mole Fraction (%)		Average NP Diameter (nm)	Maximum Wavelength (nm)
	Au	Ag		
Au	--	--	7.00 ± 0.46	521
Au_4Ag	86	14	8.04 ± 0.46	513
Au_3Ag_2	62	38	7.04 ± 0.43	475
Au_2Ag_3	41	59	8.12 ± 0.78	446
$AuAg_4$	17	83	8.09 ± 1.06	420
Ag	--	--	7.27 ± 0.58	405

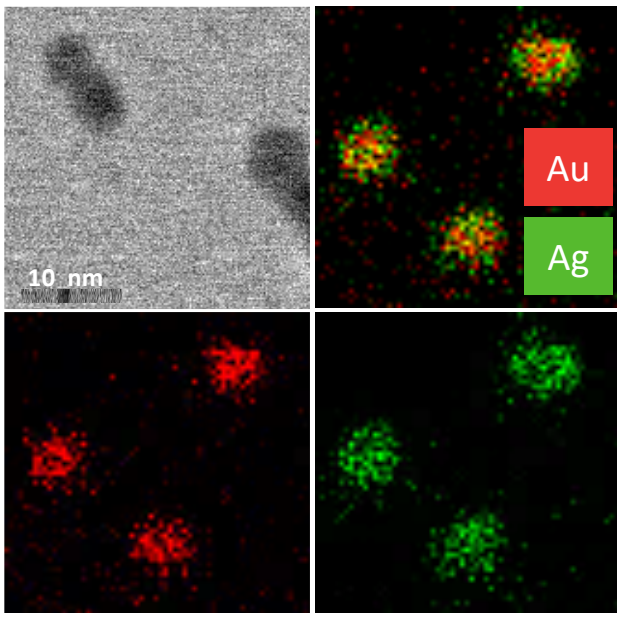

Figure 3. HRTEM image and EDS elemental mapping of Au_2Ag_3@Olam. The scale bar represents 10 nm and is applicable to all four images. Au is highlighted in red and Ag is marked by green.

Since the Au_xAg_{1-x}@Olam NPs were synthesized based on the calculated stoichiometry of the precursors, the actual metal composition of the NPs was quantitatively determined using EDS. The metal mole fraction of each alloy sample shown in **Table 2** is the average result of three measurements at different regions with a 4 % standard deviation. The measured composition is close to the expected ratio, except in $AuAg_4$, the Ag is relatively underestimated. The compositional distribution of the alloy NPs was also investigated using EDS elemental mapping. With Au_2Ag_3 NPs as the representative, the EDS maps in **Figure 3** exhibit an overlay of Ag and Au with relatively even distribution, confirming the formation of an alloy nanostructure.

UV-vis spectra of Au_xAg_{1-x}@Olam NPs in **Figure 4** show surface plasmon resonance for each sample, confirming the formation of alloy NPs. The wavelength of the distinct absorption peaks is within the range from 405 nm to 521 nm, which are characteristic of single component Ag and Au NPs, respectively. As the relative composition of Au increases, a redshift of the peaks is seen, which agrees with the observations reported in the previous articles.[1,10,11] A linear dependence of absorption maxima on the Au mole fraction (x_{Au}) is further confirmed by the diagram with a 0.99 linear regression factor shown in **Figure 5**.

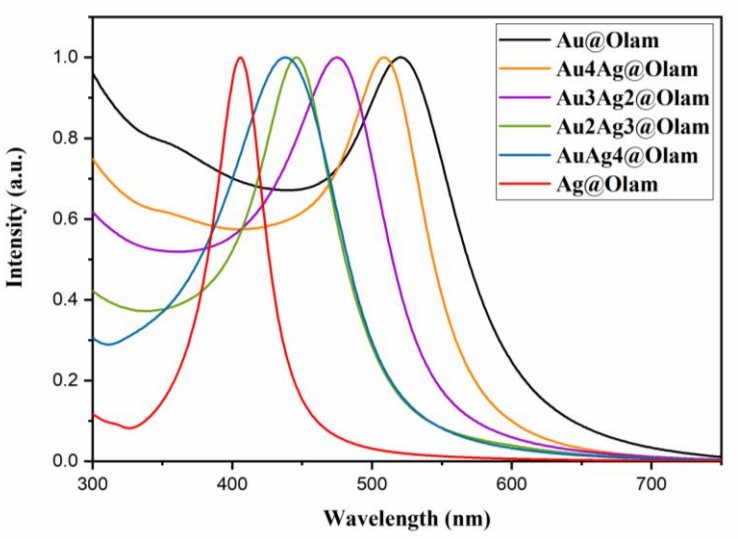

Figure 4. UV-vis spectra of Au_xAg_{1-x}@Olam NPs. The spectrum has been normalized at the absorption maxima.

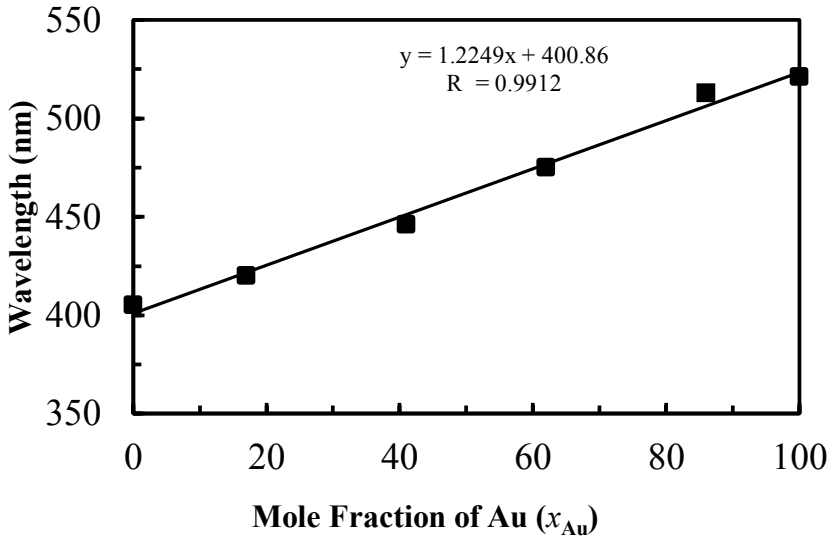

Figure 5. Wavelengths of the plasmon maxima as a function of the mole fraction of Au. The solid line represents a linear fit of the absorption maxima to x_{Au} with a 0.9912 coefficient of determination.

The ligands were grated onto the NP surface via a ligand exchange procedure, in which the weakly coordinated Olam is replaced with thiol ligands that have stronger bonding to the NPs. Since thiol ligands attach strongly to the surface of the metal NPs, addition of high concentrated ligand solution might cause irreversible deterioration to the nanostructures. Therefore, experiments employing DDT ligands were conducted and the optimized condition for the ligand exchange reactions were found, as the binding affinity of the commercially available DDT to the metal NPs is very similar to that of the anthracene containing ligand. The persistency of the size and shape of the inorganic core after ligand exchange was investigated using TEM (see **Appendix 1-3**). **Table 3** shows that all the resulting alloy NPs exhibit reasonably narrow size distribution within the range from 4 % to 18 %. The sizes of the NPs increase to varied extents compared with the original ones, which can be attributed to Oswald ripening during the exchange process. Five of the Au_xAg_{1-x}@**1** samples exhibit similar sizes which are within the range from 9 to 10 nm, except Au_3Ag_2@**1** (7.27 ± 0.67). However, the ripening of the NPs does not bring significant difference in the optical properties that the plasmon resonance peaks as a negligible shift is observed (**Table 4**). The successful replacement and complete removal of the Olam ligands in Au_xAg_{1-x}@DDT and Au_xAg_{1-x}@**2** samples were confirmed using NMR spectra, which can be found in **Appendix 19** and **20**. However, excess ligands in Au_xAg_{1-x}@**1** are relatively more difficult to remove. As seen in **Figure 6**, no peak from Olam at 5.30 ppm is observable, while peaks at 4.25, 4.8, and 7.5-8.5 ppm that belong to dendrimer **1** are present. Both evidences indicate that all the Olam ligands are replaced with ligand **1**. A relatively weak and broad peak at 2.7 ppm in **Figure 6a**, **6b** and **6e**, which is highlighted in orange, indicates that most of the ligands are bonded to the NPs. However, a sharp triplet at 2.7 ppm is seen in **Figure 6c** and **6d**, which means free ligands are still present in the solution of Au_2Ag_3 @**1** and Au_3Ag_2@**1** NPs. The NPs after ligand exchange generally exhibit improved colloidal stability compared with Au_xAg_{1-x}@Olam NPs and are robust to over five times of purification procedure without aggregation.

Table 3. The average diameter sizes of the alloy NPs after ligand exchange with DDT, 1, and 2 ligands.

Samples	Average NP Diameter (nm)			
	Olam	**DDT**	**1**	**2**
Ag	7.27 ± 0.58	7.98 ± 0.70	9.00 ± 1.62	7.89 ± 0.93
$AuAg_4$	8.09 ± 1.06	10.16 ± 1.39	10.03 ± 0.86	10.46 ± 0.96
Au_2Ag_3	8.12 ± 0.78	7.87 ± 0.56	9.47 ± 0.87	7.83 ±0.75
Au_3Ag_2	7.04 ± 0.43	7.9 ± 0.72	7.27 ± 0.67	8.34 ± 0.81
Au_4Ag	8.04 ± 0.46	8.82 ± 0.36	9.56 ± 0.56	8.38 ± 0.53
Au	7.00 ± 0.46	8.84 ± 0.37	--	8.66 ± 0.41

Table 4. The UV-vis absorption maxima of Au_xAg_{1-x}@Olam, Au_xAg_{1-x}@DDT, Au_xAg_{1-x}@1, and Au_xAg_{1-x}@2 NPs.

Samples	Absorption Wavelength (nm)			
	Olam	DDT	1	2
Ag	405	422	420	414
AuAg4	420	438	431	426
Au2Ag3	446	458	460	452
Au3Ag2	475	488	489	484
Au4Ag	513	519	519	515
Au	521	525	--	522

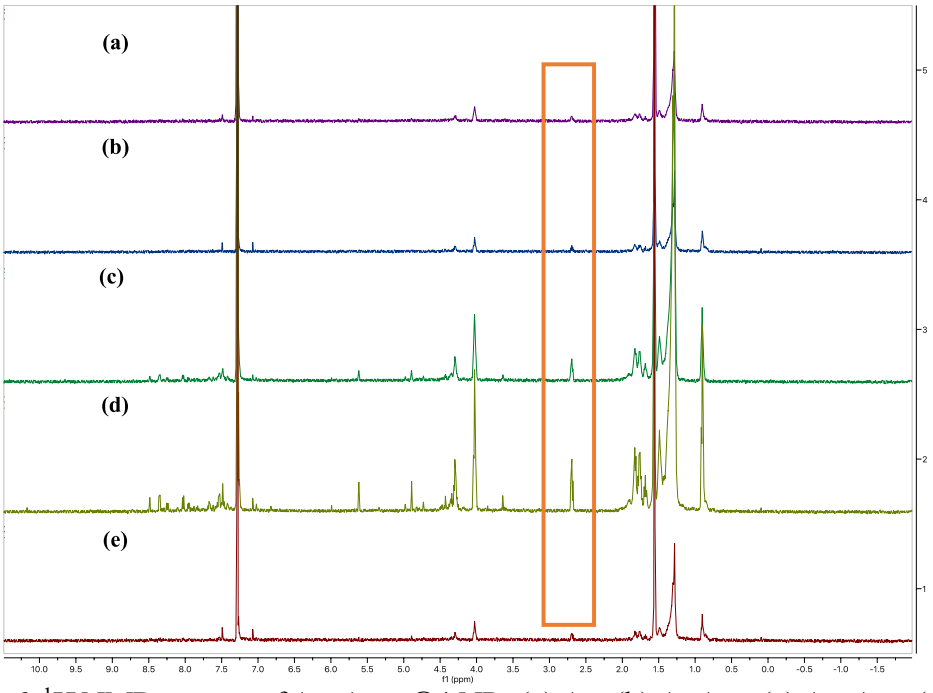

Figure 6. ^{1}H NMR spectra of Au_xAg_{1-x}@**1** NPs (a) Ag, (b) $AuAg_4$, (c) Au_2Ag_3, (d) Au_3Ag_2, (e) Au_4Ag.

The UV-vis and fluorescence spectra are summarized in **Figure 7**, with Ag@**1**, $AuAg_4$@**1**, Au_2Ag_3@**1**, Au_3Ag_2@**1**, and Au_4Ag@**1** highlighted in red, blue, green, purple and orange, respectively. As seen in the UV-vis spectrum (**Figure 7a**), anthracene exhibits a broad absorption band ranging from ca. 330 to 400 nm in each sample. The intensity of the anthracene absorption varies among the five samples, which may be due to different enhancement of light absorbing ability induced by the metal core. Variance in surface coverage of the ligands as well as excess ligands remaining in the solution might also result in discrepancy in the measure of fluorescence.

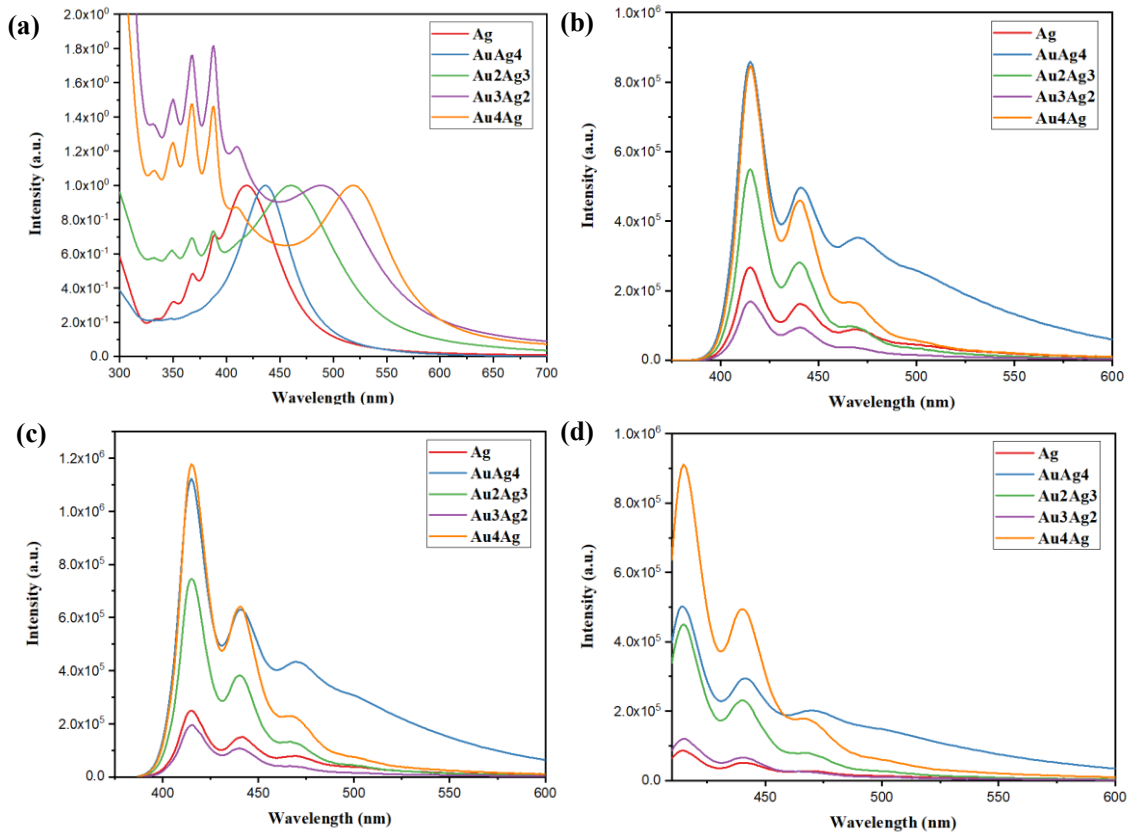

Figure 7. UV-vis and fluorescence spectra of Au_xAg_{1-x}@**1** NPs. (a) UV-vis, (b)(c)(d) fluorescence spectra with NPs excited at 350 nm, 367 nm, and 390 nm, respectively. The UV-vis spectra were normalized at the absorption maxima. Fluorescence spectra were also rescaled according to the UV-vis and normalized at the excited wavelength.

Au_xAg_{1-x} @**1** NPs were excited at three different wavelengths, which are 350 nm, 367 nm and 390 nm, respectively, according to the three absorption maxima of the anthracene molecule. The fluorescence spectrum of **1** consists of three emission peaks at maximum wavelength 415, 440 and 470 nm and an additional broad peak at around 500 nm. The recorded emission wavelengths remain the same no matter what the exciting light was used, despite of the fluorescence intensity. The emission band shows a red shift compared with the absorption band and resembles a mirror image of the absorption caused by Stokes shift. For all the samples, the most intense emission occurs when the they were excited at 367 nm. The fluorescence intensity of the samples at 350 nm excitation follows a descending order for Au_4Ag, $AuAg_4$, Au_2Ag_3, Ag and Au_3Ag_2 NPs. Interestingly, as the spectral overlap between the plasmon band and the absorption/emission bands of the anthracene decreases among Ag, $AuAg_4$, Au_2Ag_3, Au_3Ag_2, and Au_4Ag, the expected fluorescence intensity should follow the same sequence. However, a disordered trend was observed. There are several reasons to explain this phenomenon. The first one is the variance in the light absorption of the anthracene. It is possible that anthracene in free ligands also contribute to a portion in absorbing light compared with the coupled fluorophore while emits light less efficiently. Since the spacing between the metal and the fluorophore plays

an important role in emission efficiency, direct contact of the NPs with the anthracene may lead to a fluorescence quenching instead of an enhancement effect. To further study the plasmonic effect of the alloy NPs, more work needs to be done including understanding the difference in light absorption of the samples and determining the exact absorption efficiency and emission efficiency of the NP-coupled anthracene. To achieve this, fluorescence spectra of pure anthracene ligand (**Figure 8**) can be obtained to quantitatively investigate the fluorescence enhancement. Additionally, the effect of the absorption or emission of the ligand, with anthracene excluded, should also be investigated by recording the UV-vis and fluorescence spectra of control ligand **2**.

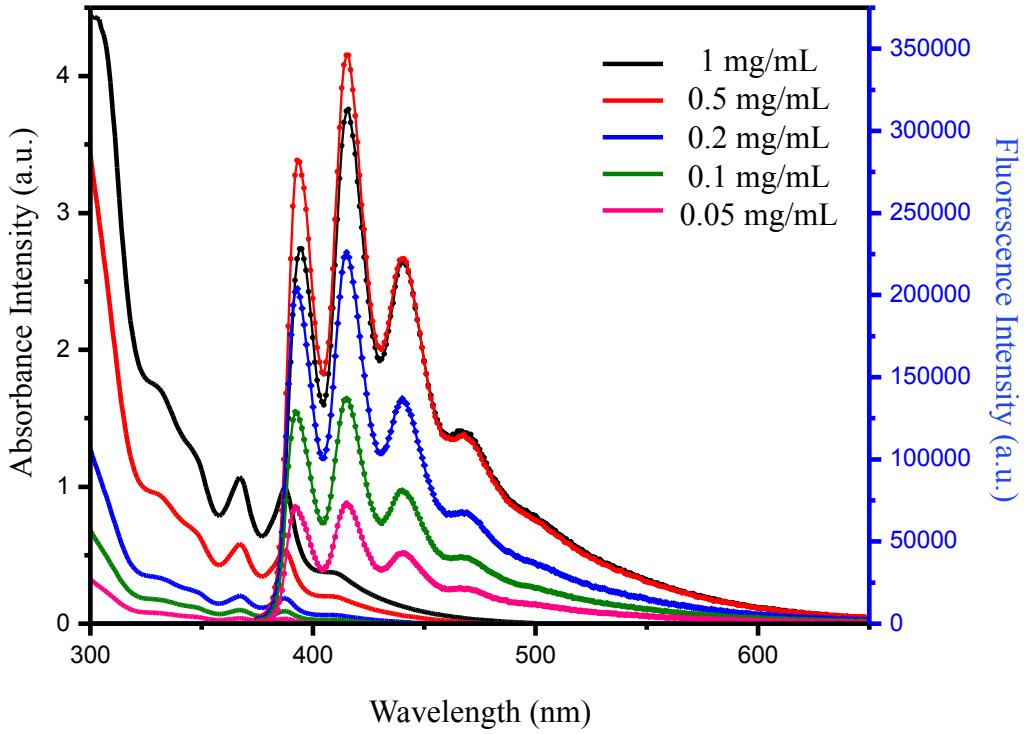

Figure 8. UV-vis and fluorescence spectra of pure anthracene ligand at different concentrations. The concentrations of samples marked by black, red, blue, green, and pink are 1 mg/mL, 0.5 mg/mL, 0.2 mg/mL, 0.1 mg/mL, and 0.05 mg/mL, respectively.

Conclusion and Future Work

In summary, relatively homogeneous Au-Ag alloy spherical NPs were synthesized and functionalized with an anthracene-containing ligand. The average size of Au_xAg_{1-x}@**1** NPs is 9 nm in diameter. The plasmonic effect of the fluorescence was investigated to be varied among different compositions of the alloy NPs, but also dependent on other factors which includes the dimension of the metal cores and surface coverage of the NPs.

More work could be done including optimization of the reaction time or chemical reagents to synthesize more uniform Au-Ag alloy NPs that are chemically and structurally stable over time. Other techniques, including inductively coupled plasma spectroscopy (ICP) can be used towards more quantitative measure of the elemental composition. Ligand exchange process should be controlled to prevent too much ripening of the NP, in order to yield NPs with minimal polydispersity. A better purification procedure can be adopted to remove all the excess ligands without destroying the NPs. Additionally, fluorescence spectra of pure anthracene molecule and anthracene-embedded ligands could be taken for reference. Further research can be also conducted on different topics based on varied material systems, for instance, to investigate how the dimension or morphology of the NPs, the spatial distance between the fluorophore and the metal core, or the anisotropy of the NPs affect the fluorescence efficiency.

References

1. Link, S.; Wang, Z. L.; El-Sayed, M. A. Alloy Formation of Gold−Silver Nanoparticles and the Dependence of the Plasmon Absorption on Their Composition. *J. Phys. Chem. B* **1999**, *103*, 3529–3533.
2. Sokolov, K.; Chumanov, G.; Cotton, T. M. Enhancement of Molecular Fluorescence near the Surface of Colloidal Metal Films. *Anal. Chem.* **1998**, *70*, 3898–3905.
3. Bardhan, R.; Grady, N. K.; Cole, J. R.; Joshi, A.; Halas, N. J. Fluorescence Enhancement by Au Nanostructures: Nanoshells and Nanorods., *ACS Nano.* **2009**, *3*, 744–752.
4. Wang, D.-S.; Kerker, M. Absorption and Luminescence of Dye-Coated Silver and Gold Particles. *Phys. Rev. B* **1982**, *25*, 2433–2449.
5. Amendola, V.; Pilot, R.; Frasconi, M. Surface Plasmon Resonance in Gold Nanoparticles: A Review., *J. Phys. Condens. Matter.* **2017**, *29*, 1–17.
6. Elbert, K. C.; Jishkariani, D.; Wu, Y.; Lee, J. D.; Donnio, B.; Murray, C. B. Design, Self- Assembly, and Switchable Wettability in Hydrophobic, Hydrophilic, and Janus Dendritic Ligand-Gold Nanoparticle Hybrid Materials., *Chem. Matter.* **2017**, *29*, 8737–8746.
7. Schmelzeisen, M.; Zhao, Y.; Klapper, M.; Mu, K.; Kreiter, M. Fluorescence Enhancement from Individual Plasmonic Gap Resonances., *J. Nanobiotechnology.* **2010**, *4*, 3309–3317.
8. Yu, H.; Peng, Y.; Yang, Y.; Li, Z. Plasmon-Enhanced Light–Matter Interactions and Applications. *npj Comput. Mater.* **2019**, *5*, 1–14.
9. Smetana A. B.; Klabunde K. J.; Sorensen C. M.; Ponce A. A.;, and, and Mwale B. Low-Temperature Metallic Alloying of Copper and Silver Nanoparticles with Gold Nanoparticles through Digestive Ripening., *The Journal of Physical Chemistry B*, **2006**, *110*, 2155–2158.
10. Yang, H.; Wong, E.; Zhao, T.; Lee, J. D.; Xin, H. L.; Chi, M.; Fleury, B.; Tang, H.-Y.; Gaulding, E. A.; Kagan, C. R.; et al. Charge Transport Modulation in PbSe Nanocrystal Solids by AuxAg1–x Nanoparticle Doping. *ACS Nano* **2018**, *12*, 9091–9100.
11. Blaber, M. G.; Arnold, M. D.; Ford, M. J. A Review of the Optical Properties of Alloys and Intermetallics for Plasmonics. *J. Phys. Condens. Matter* **2010**, *22*, 1–5.
12. Stranik, O.; McEvoy, H. M.; McDonagh, C.; MacCraith, B. D. Plasmonic Enhancement of Fluorescence for Sensor Applications. *Sensors Actuators B Chem.* **2005**, *107*, 148–153.
13. Santosh, G.; Shirman, E.; Weissman, H.; Shimoni, E.; Pinkas, I.; Rudich, Y.; Rybtchinski, B. Photofunctional Self-Assembled Nanostructures Formed by Perylene Diimide−Gold Nanoparticle Hybrids. *J. Phys. Chem. B* **2010**, *114*, 14389–14396.
14. Jayabharathi, J.; Sundari, G.; Thanikachalam, V.; Jeeva, P.; Panimozhi, S. A Dodecanethiol-Functionalized Ag Nanoparticle-Modified ITO Anode for Efficient Performance of Organic Light-Emitting Devices. *RSC Adv.* **2017**, *7*, 38923–38934.

15. Elbert, K. C.; Lee, J. D.; Wu, Y.; Murray, C. B. Improved Chemical and Colloidal Stability of Gold Nanoparticles through Dendron Capping., *Langmuir* **2018**, *34*, 13333–13338.
16. Chandross, E. A.; Ferguson, J.; McRae, E. G. Absorption and Emission Spectra of Anthracene Dimers. *J. Chem. Phys.* **1966**, *45*, 3546–3553.
17. Abdel-Mottaleb, M. S. A.; Galal, H. R.; Dessouky, A. F. M.; El-Naggar, M.; Mekkawi, D.; Ali, S. S.; Attya, G. M. Fluorescence and Photostability Studies of Anthracene-9-Carboxylic Acid in Different Media. *Int. J. Photoenergy* **2000**, *2*, 47–53.
18. Jishkariani, D.; Elbert, K. C.; Wu, Y.; Lee, J. D.; Hermes, M.; Wang, D.; van Blaaderen, A.; Murray, C. B. Nanocrystal Core Size and Shape Substitutional Doping and Underlying Crystalline Order in Nanocrystal Superlattices. *ACS Nano* **2019**, *13*, 5712–5719.
19. Peng, S.; McMahon, J. M.; Schatz, G. C.; Gray, S. K.; Sun, Y. Reversing the Size-Dependence of Surface Plasmon Resonances. *Proc. Natl. Acad. Sci.* **2010**, *107*, 14530–14534.

Appendices

Appendix 1. TEM images of Au_xAg_{1-x}@DDT NPs (a) Ag (7.98 ± 0.70 nm), (b) $AuAg_4$ (10.16 ± 1.39 nm), (c) Au_2Ag_3 (7.87 ± 0.56 nm), (d) Au_3Ag_2 (7.9 ± 0.72 nm), (e) Au_4Ag (8.82 ± 0.36 nm), (f) Au (8.84 ± 0.37 nm).

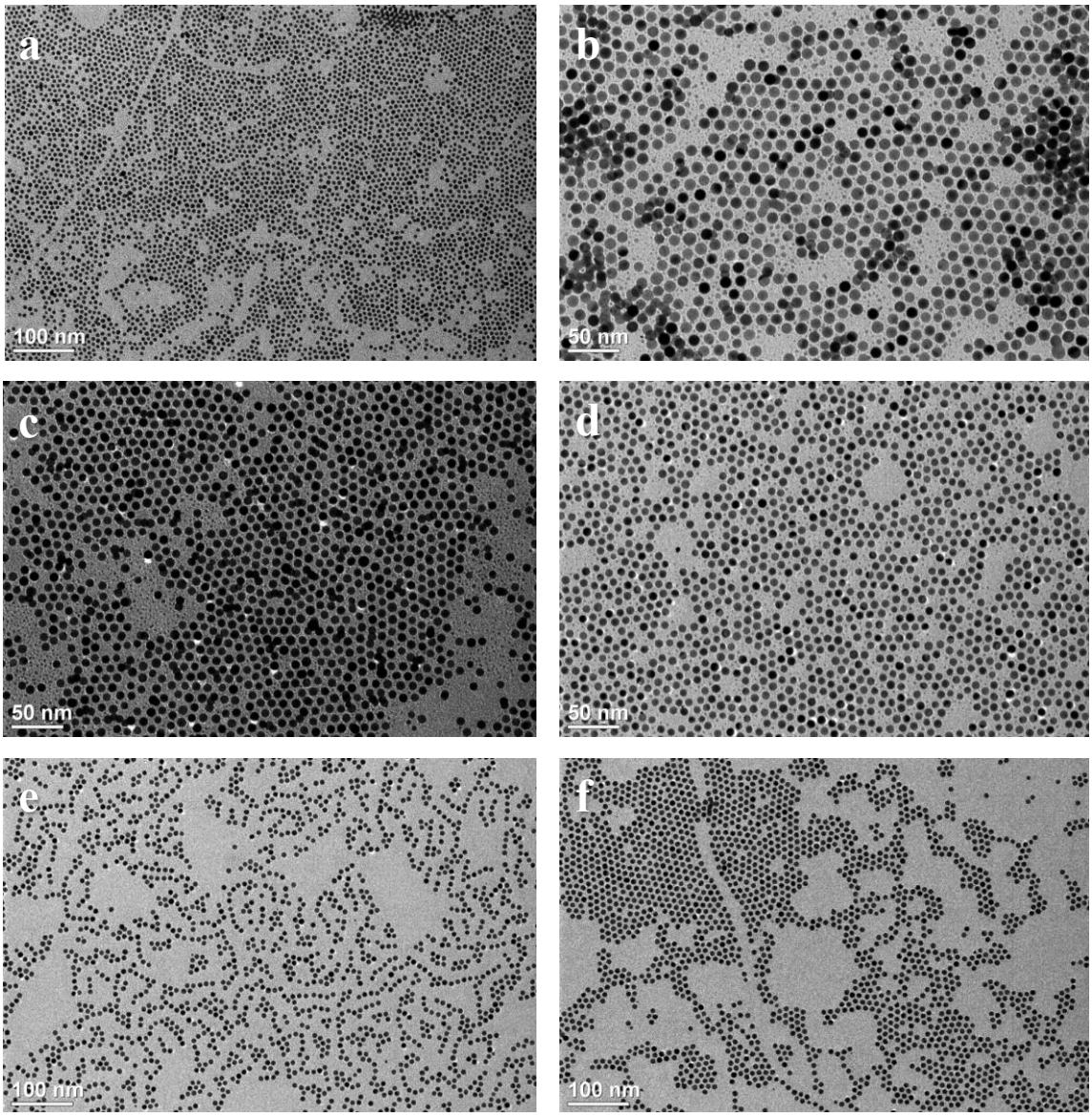

Appendix 2. TEM images of Au_xAg_{1-x}@**1** NPs (a) Ag (9.00 ± 1.62 nm), (b) $AuAg_4$ (10.03 ± 0.86 nm), (c) Au_2Ag_3 (9.47 ± 0.87 nm), (d) Au_3Ag_2 (7.27 ± 0.67 nm), (e) Au_4Ag (9.56 ± 0.56 nm).

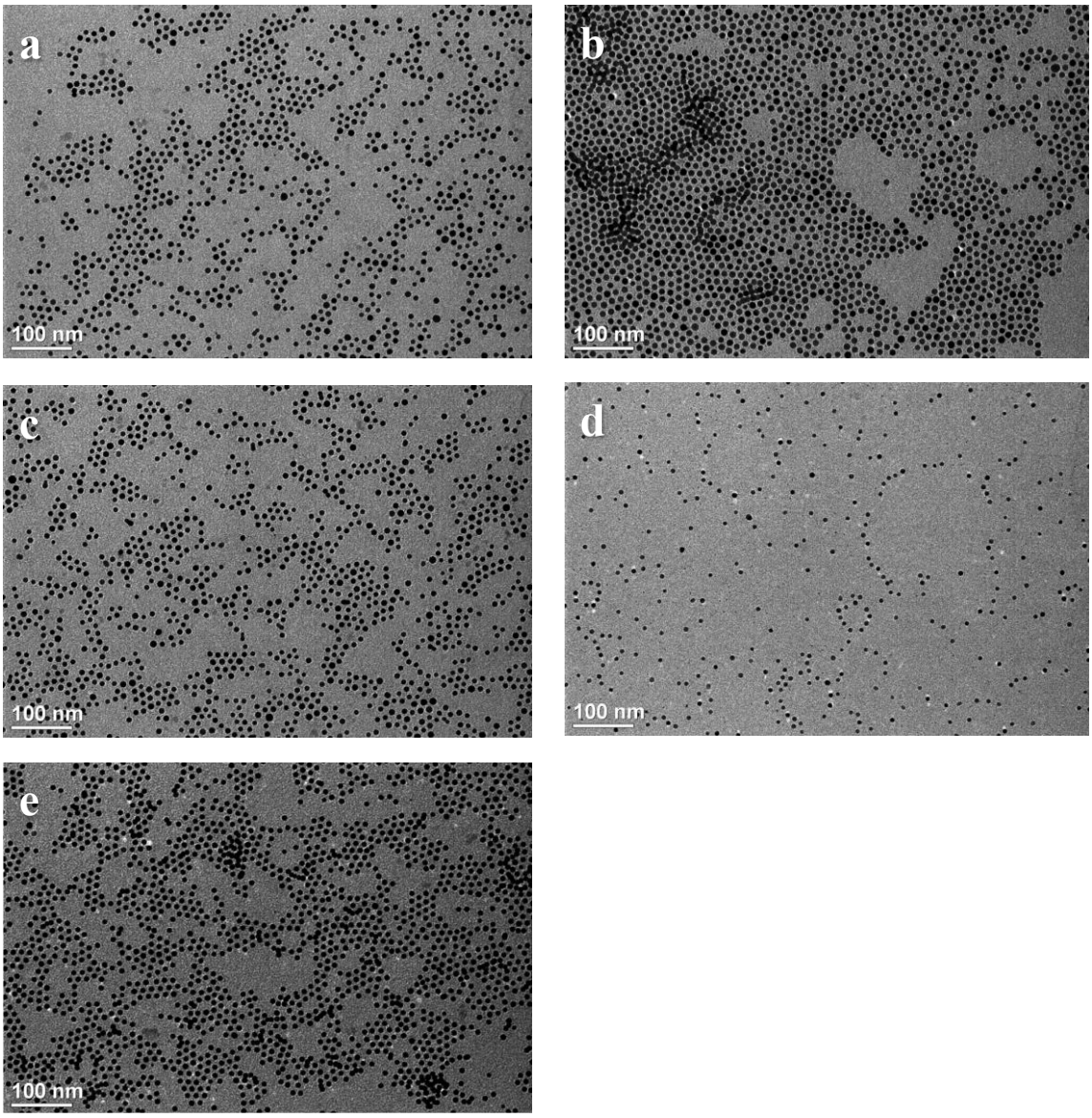

Appendix 3. TEM images of Au_xAg_{1-x}@**2** NPs (a) Ag (7.89 ± 0.93 nm), (b) $AuAg_4$ (10.46 ± 0.96 nm), (c) Au_2Ag_3 (7.83 ±0.75 nm), (d) Au_3Ag_2 (8.34 ± 0.81 nm), (e) Au_4Ag (8.38 ± 0.53 nm), (f) Au (8.66 ± 0.41 nm).

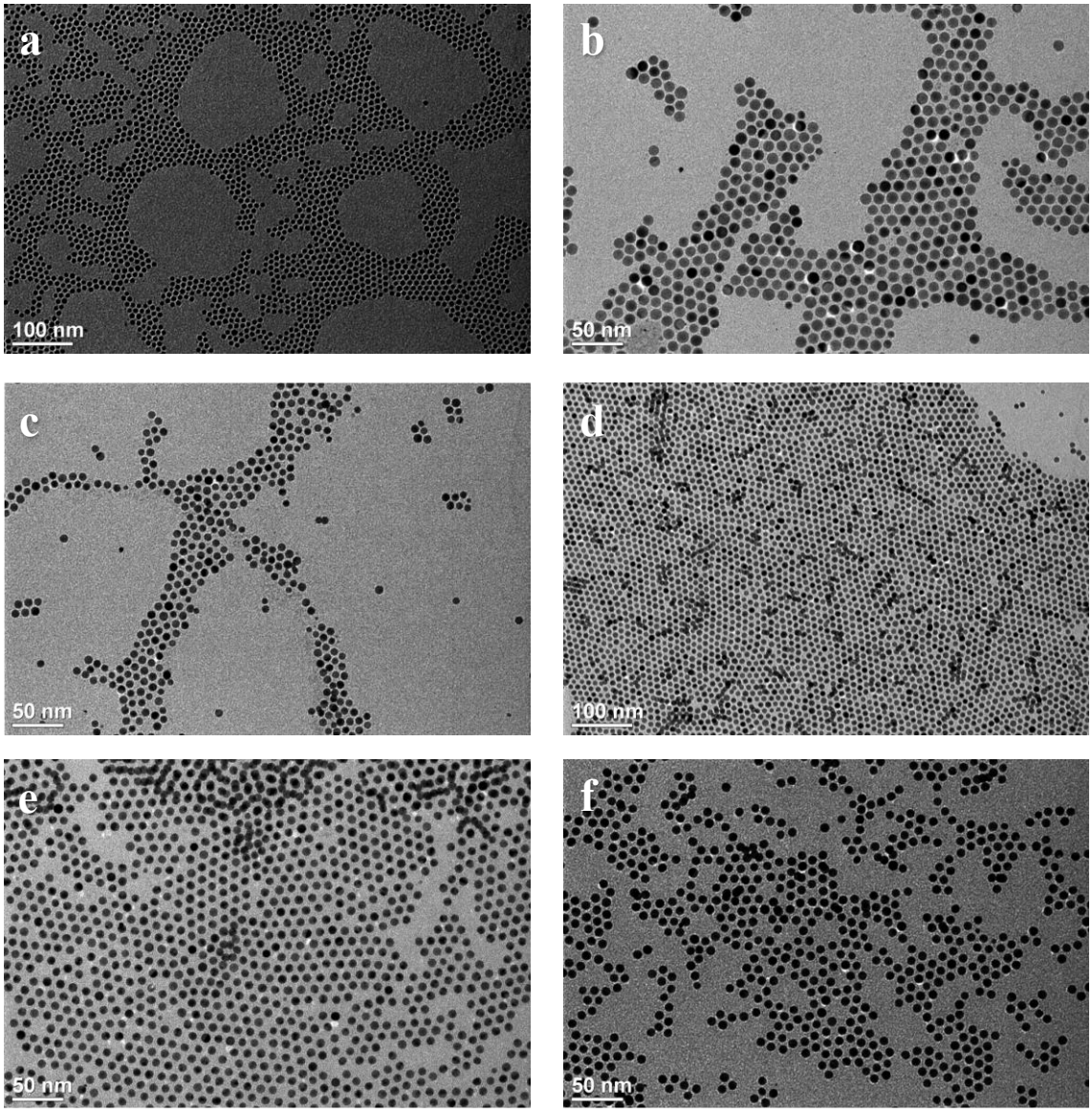

Appendix 4. Size distribution histograms of Au_xAg_{1-x}@Olam NPs (a) $AuAg_4$ (b) Au_2Ag_3, (c) Au_3Ag_2, (d) Au_4Ag alloy NPs; (e) Ag (f) Au.

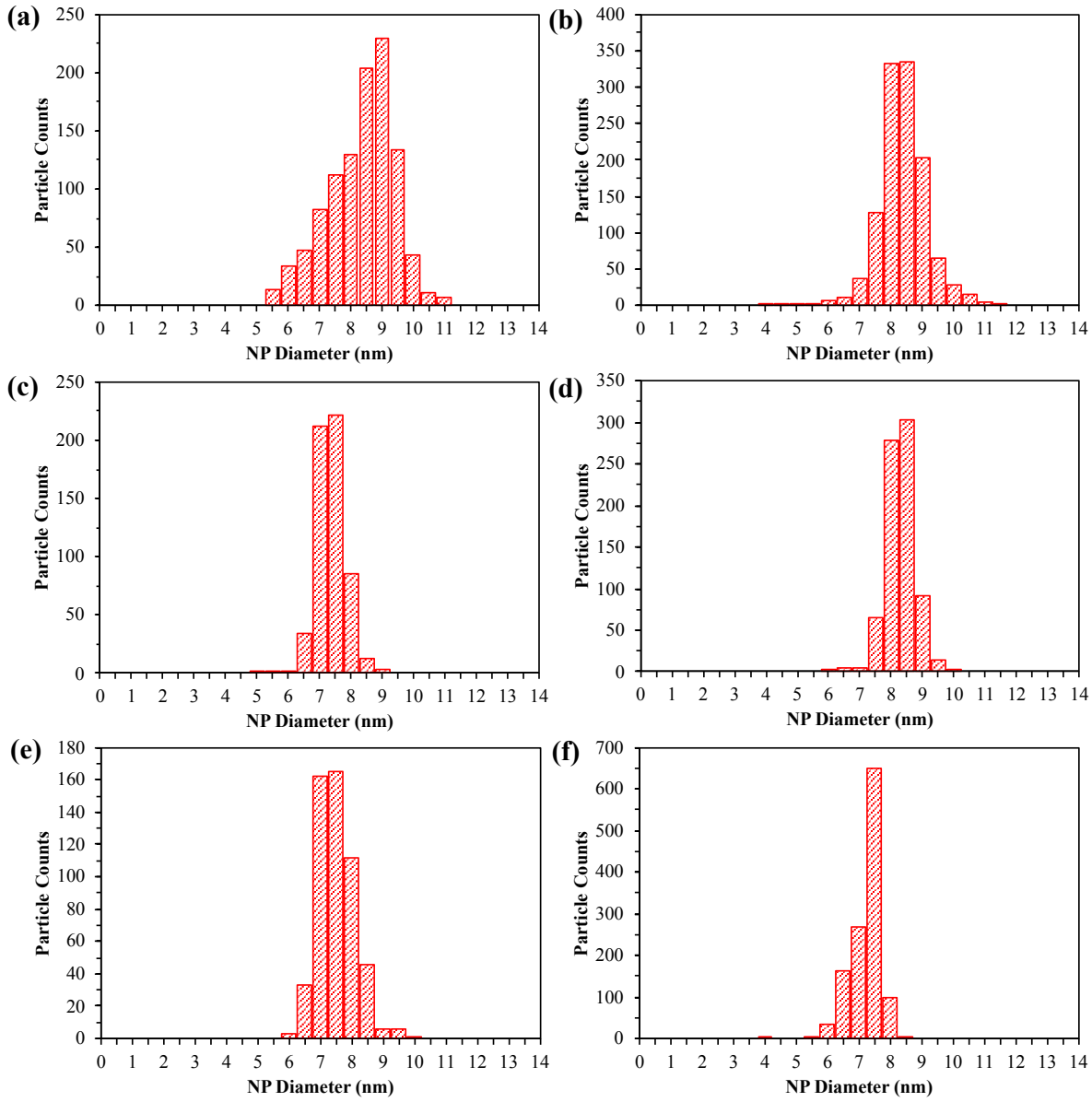

Appendix 5. Size distribution histograms of Au_xAg_{1-x}@DDT NPs (a) $AuAg_4$, (b) Au_2Ag_3, (c) Au_3Ag_2, (d) Au_4Ag, (e) Ag, (f) Au.

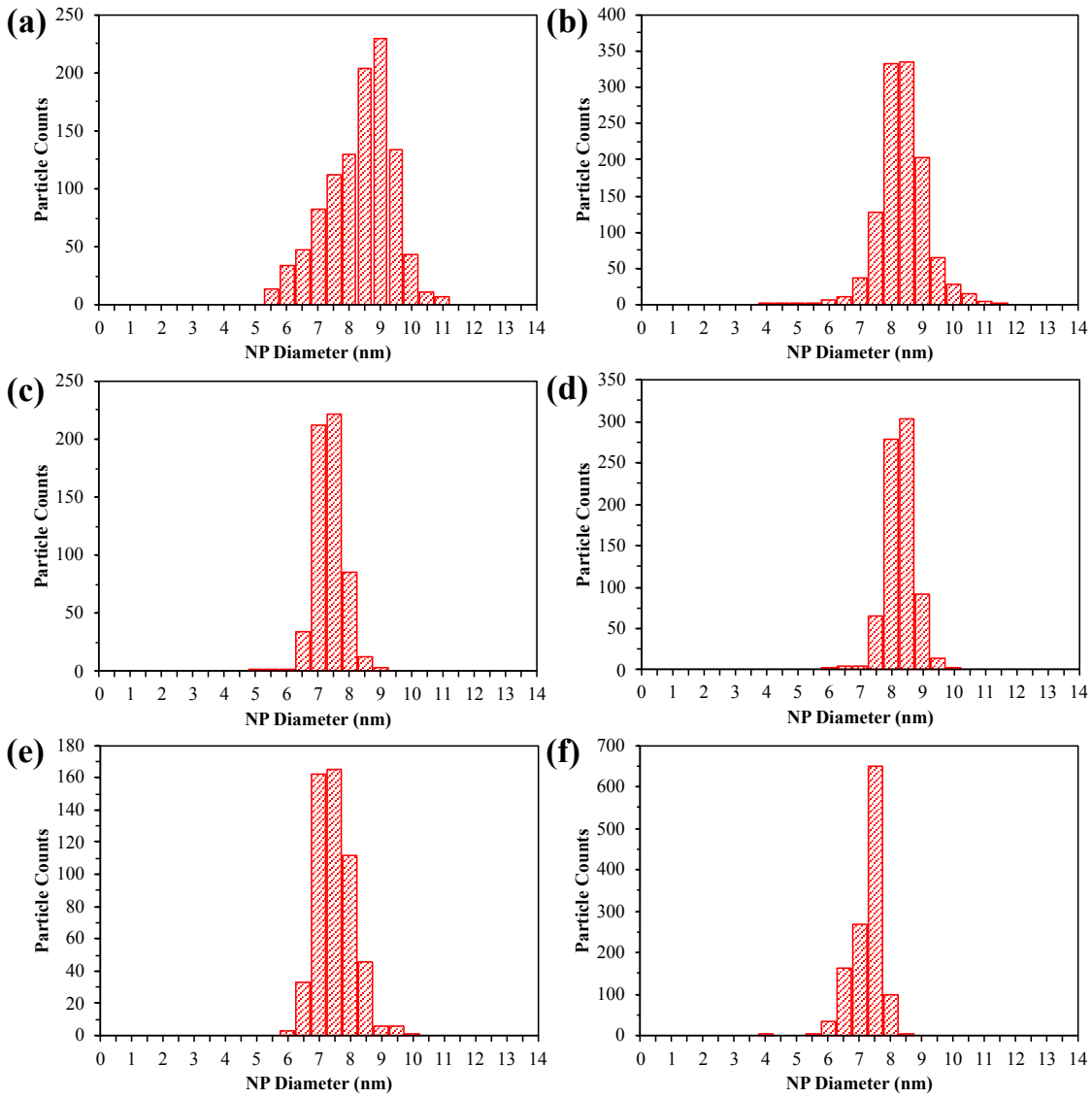

Appendix 6. Size distribution histograms of Au_xAg_{1-x}@**1** NPs (a) $AuAg_4$, (b) Au_2Ag_3, (c) Au_3Ag_2, (d) Au_4Ag, (e) Ag.

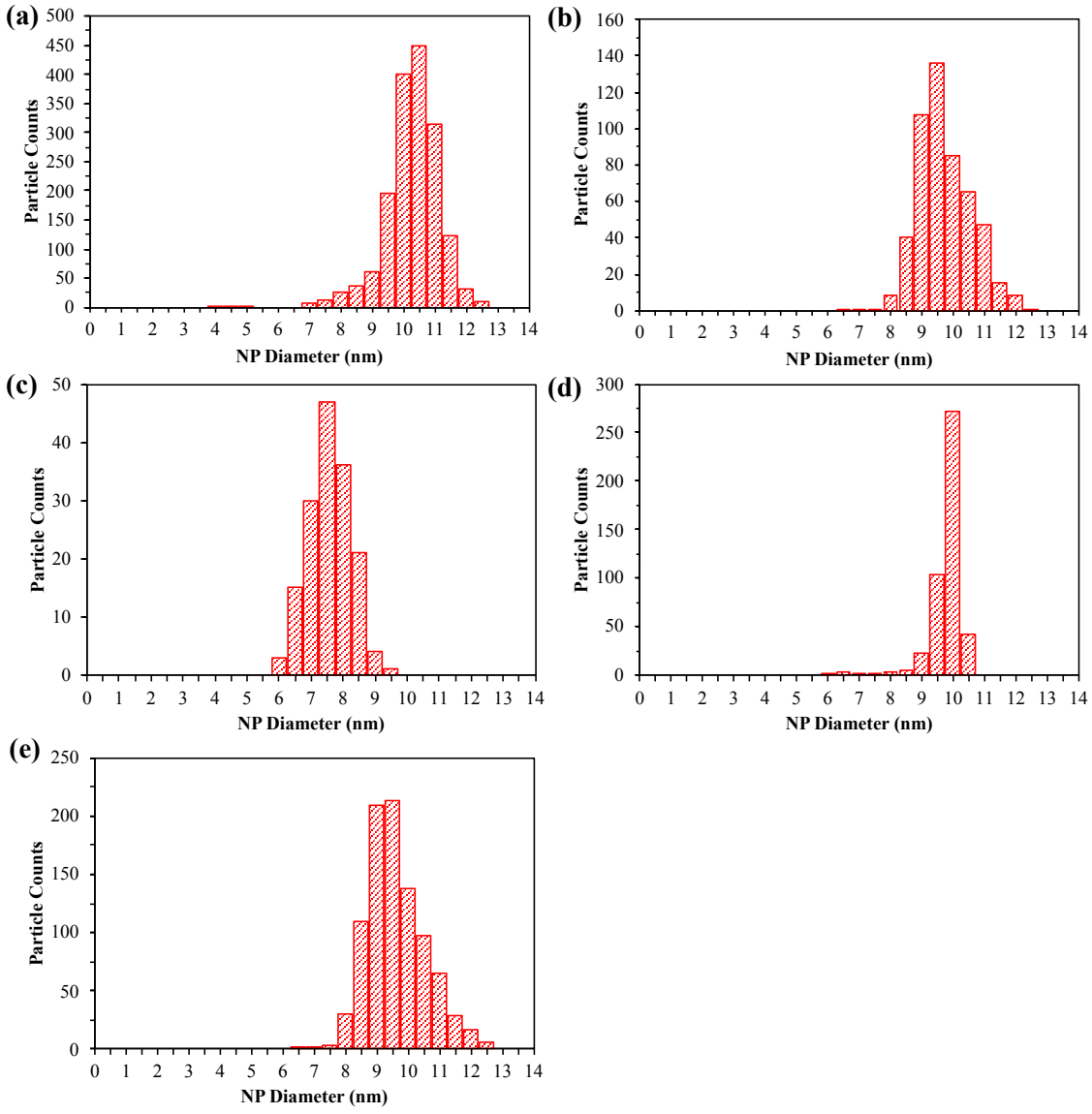

Appendix 7. Size distribution histograms of Au_xAg_{1-x}@**2** NPs (a) $AuAg_4$, (b) Au_2Ag_3, (c) Au_3Ag_2, (d) Au_4Ag, (e) Ag, (f) Au.

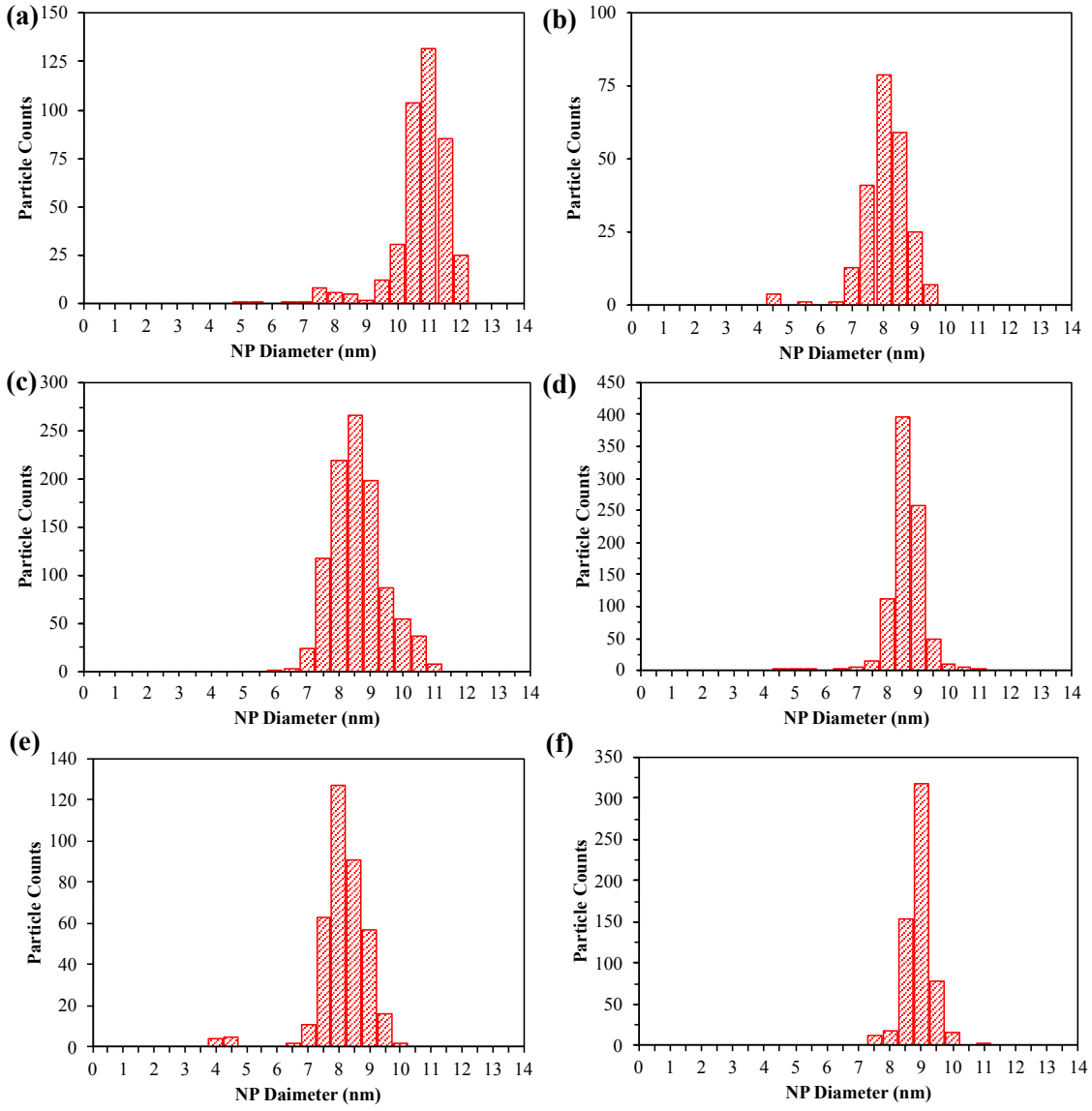

Appendix 8. XRD patterns of Au_xAg_{1-x}@Olam NPs. Intensity not on the exact scale.

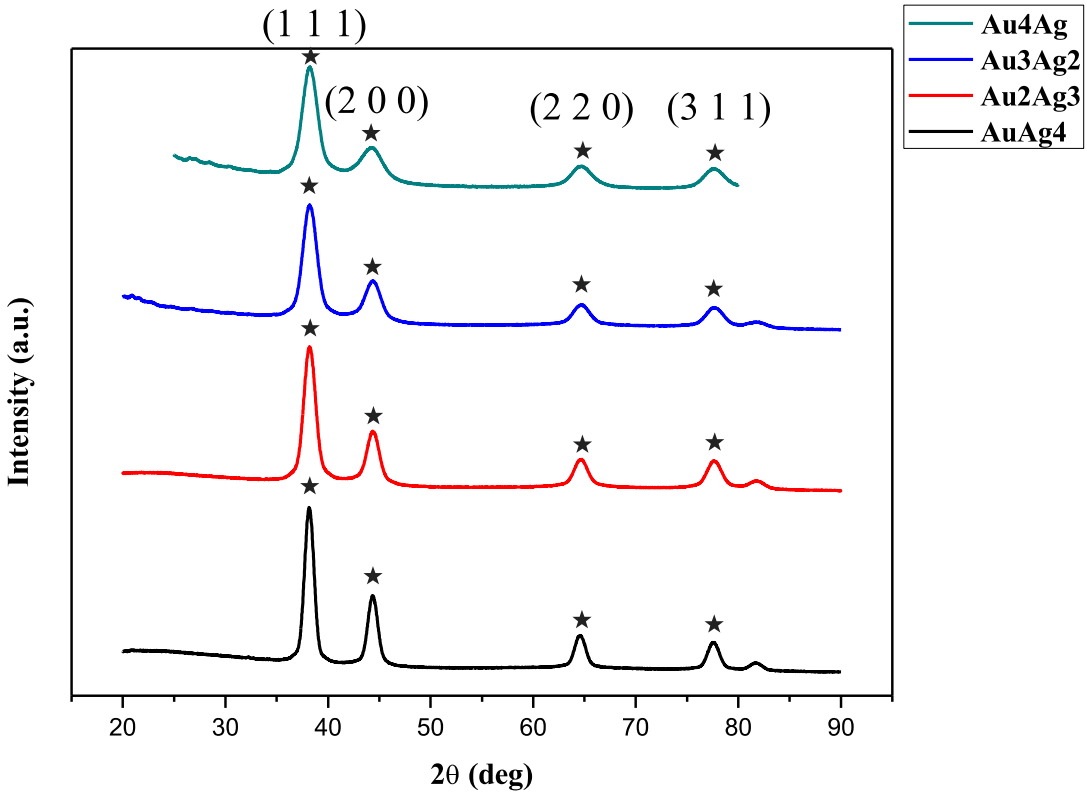

Appendix 9. EDS spectra of Au_xAg_{1-x}@Olam NPs. (a) $AuAg_4$, (b) Au_2Ag_3, (c) Au_3Ag_2, (d) Au_4Ag.

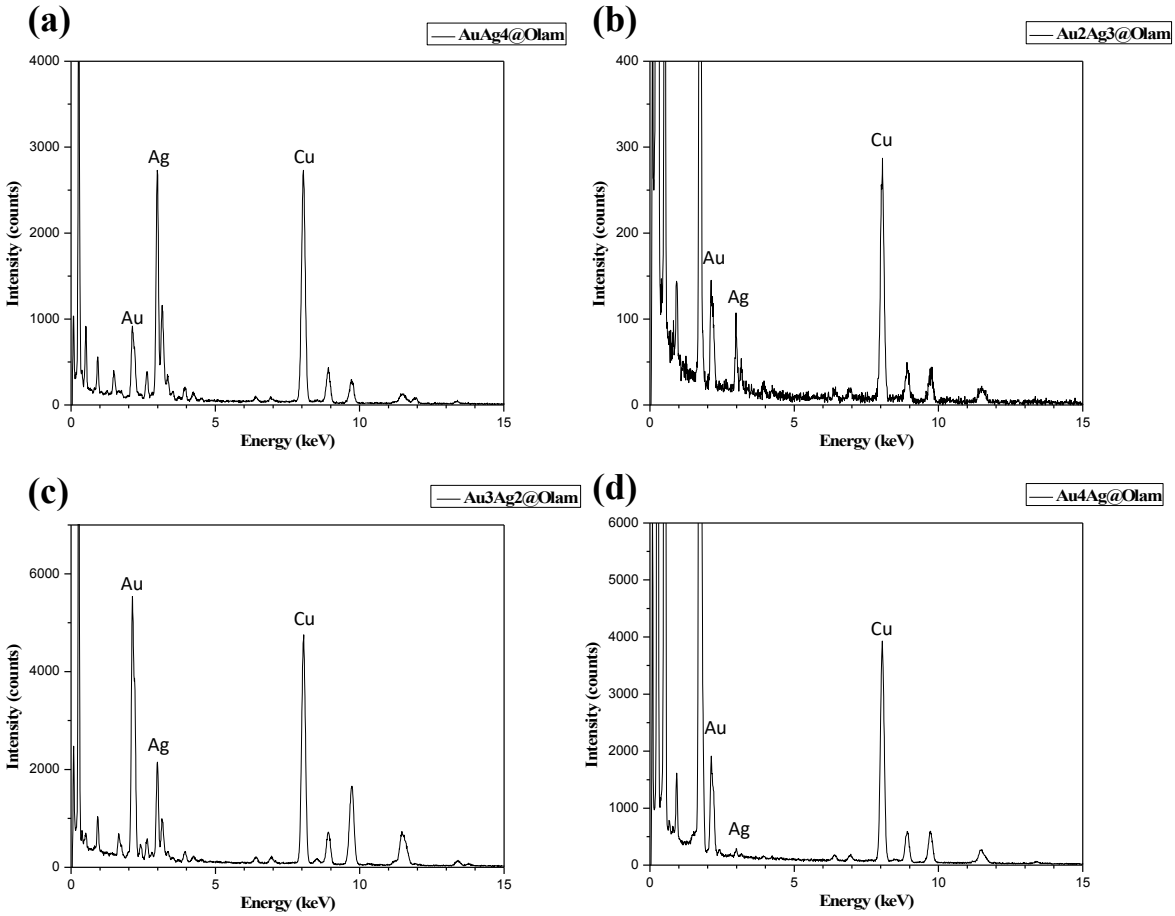

Appendix 10. STEM images of Au_4Ag@Olam NPs. (a)(d) Bright-field (BF) (b)(c) High-angle annular dark-field (HAADF) images.

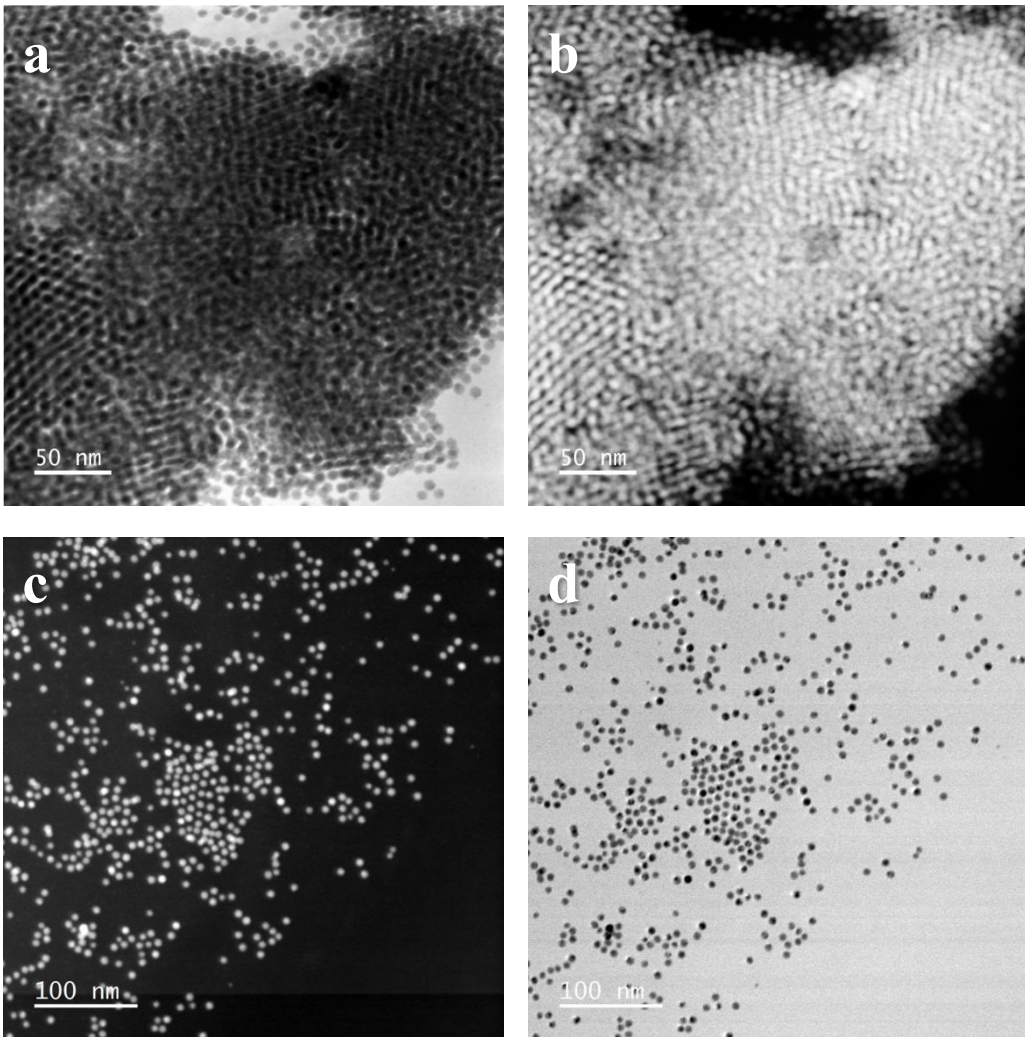

Appendix 11. STEM images of Au_3Ag_2@Olam NPs. (a)(d) BF (b)(c) HAADF images.

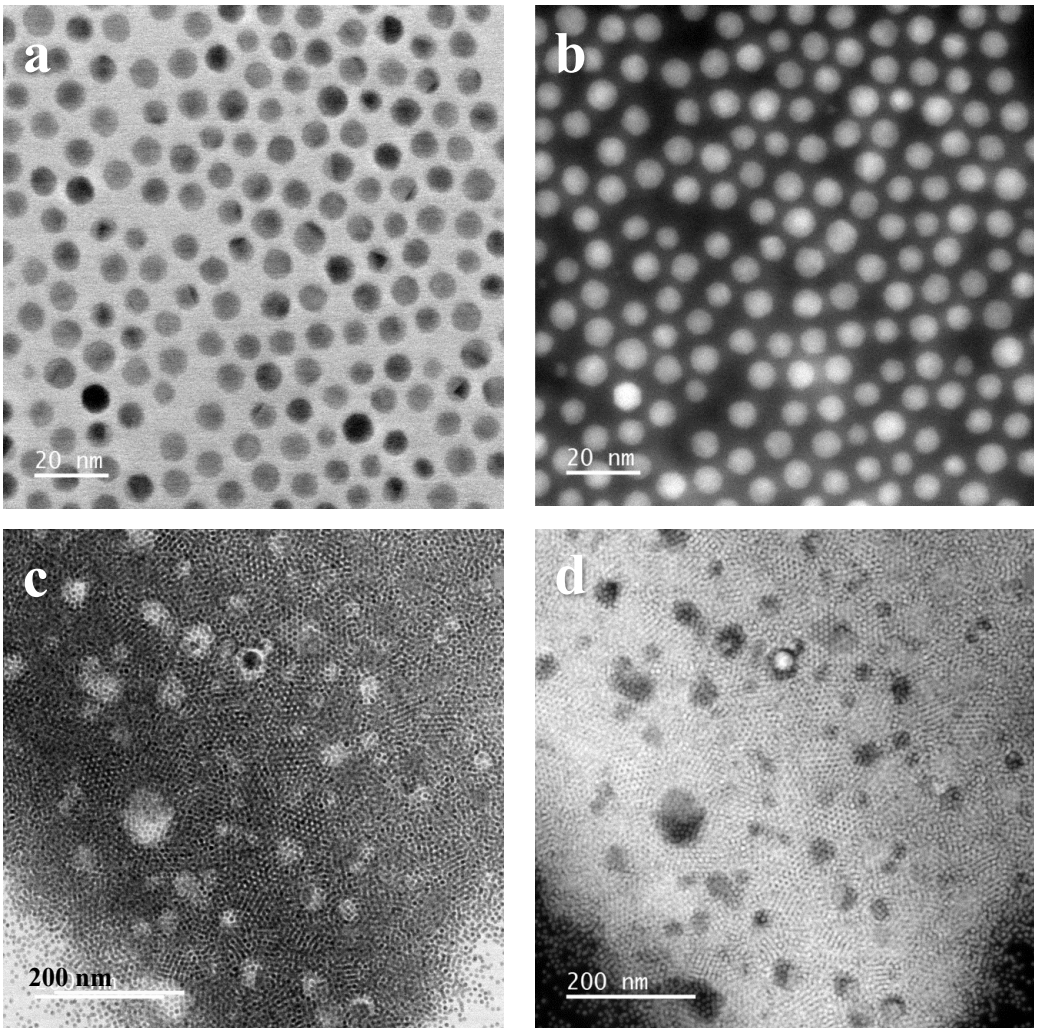

Appendix 12. HRTEM and EDS mapping of $AuAg_4$@Olam NPs. Au is highlighted in red and Ag is marked by green.

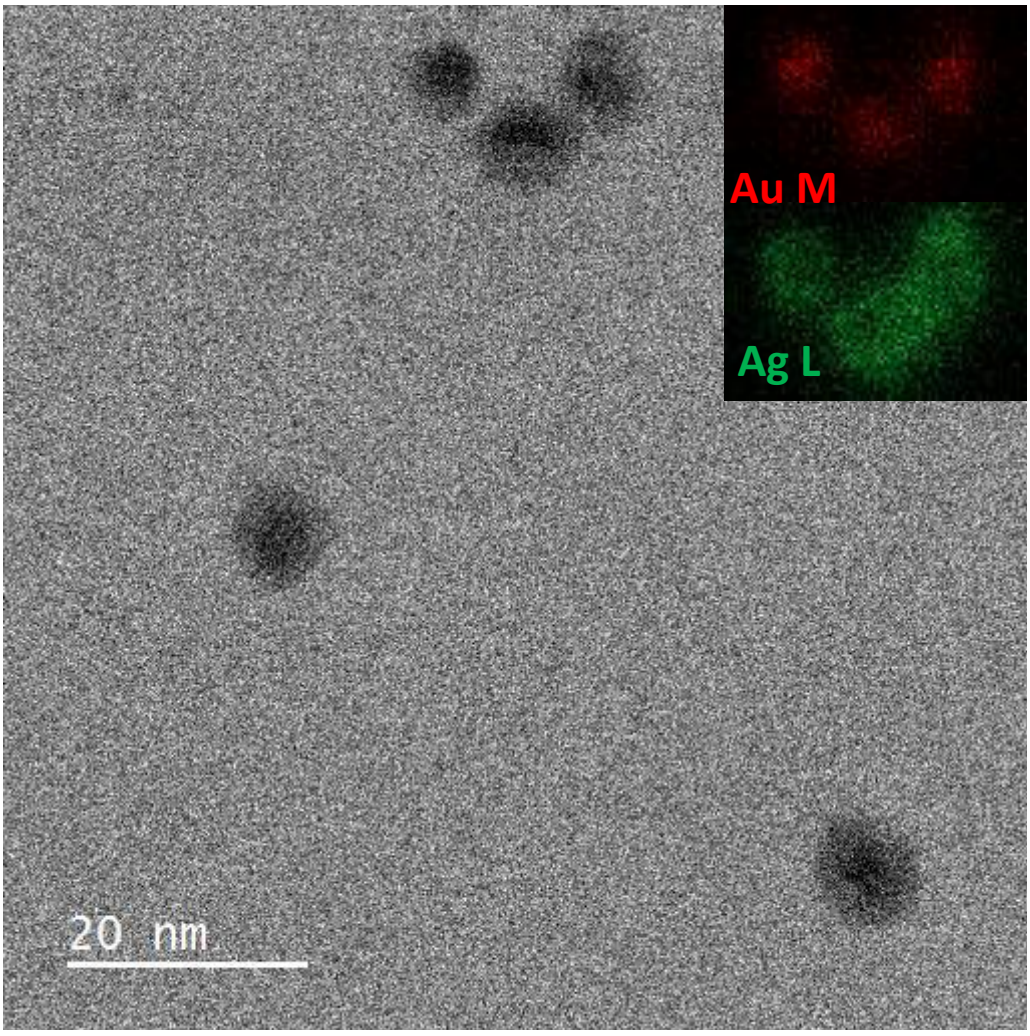

Appendix 13. EDS mapping of Au_4Ag@Olam NPs. Au is highlighted in red and Ag is marked by green. The scale bar represents 10 nm and is applicable to all four images.

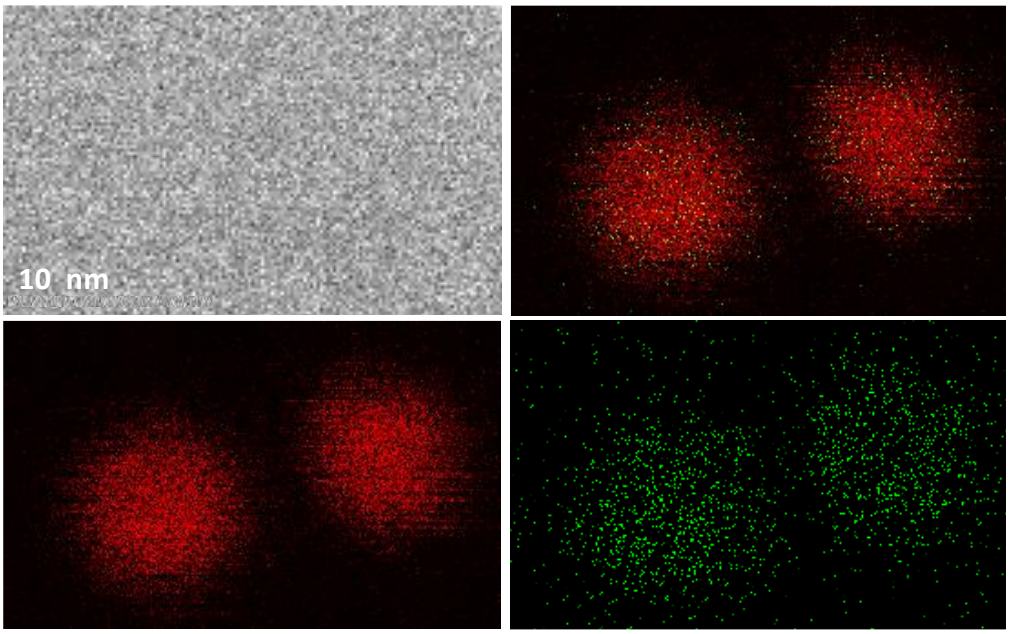

Appendix 14. UV-vis spectra of Au_xAg_{1-x}@DDT NPs. The spectrum has been normalized at the absorption maxima.

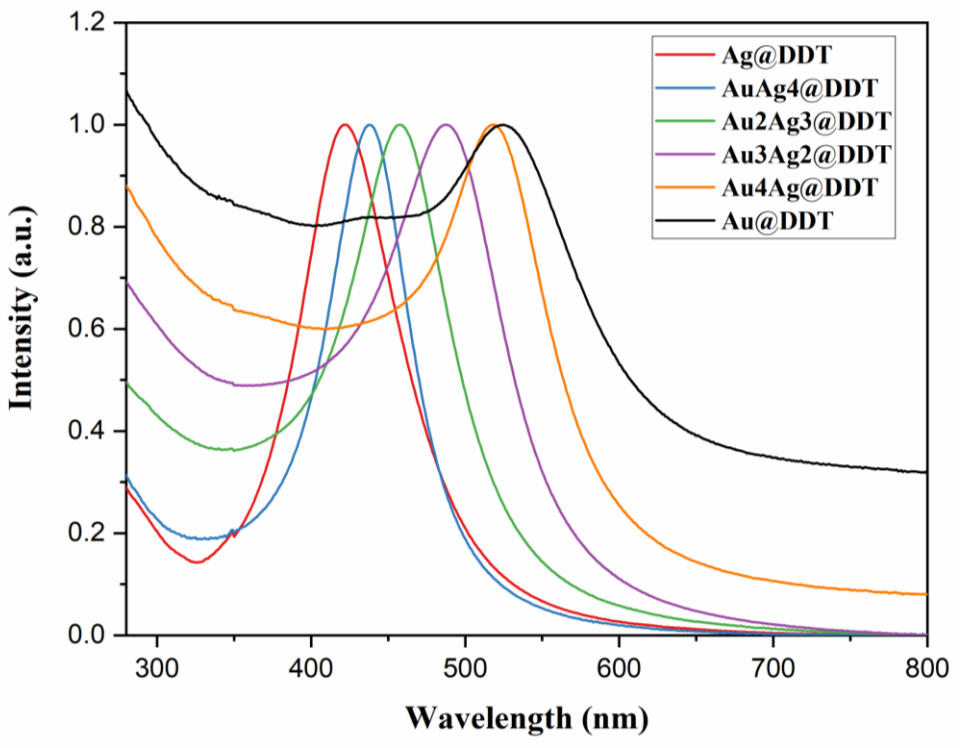

Appendix 15. UV-vis spectra of Au_xAg_{x-1}@**2** NPs. The spectrum has been normalized at the absorption maxima.

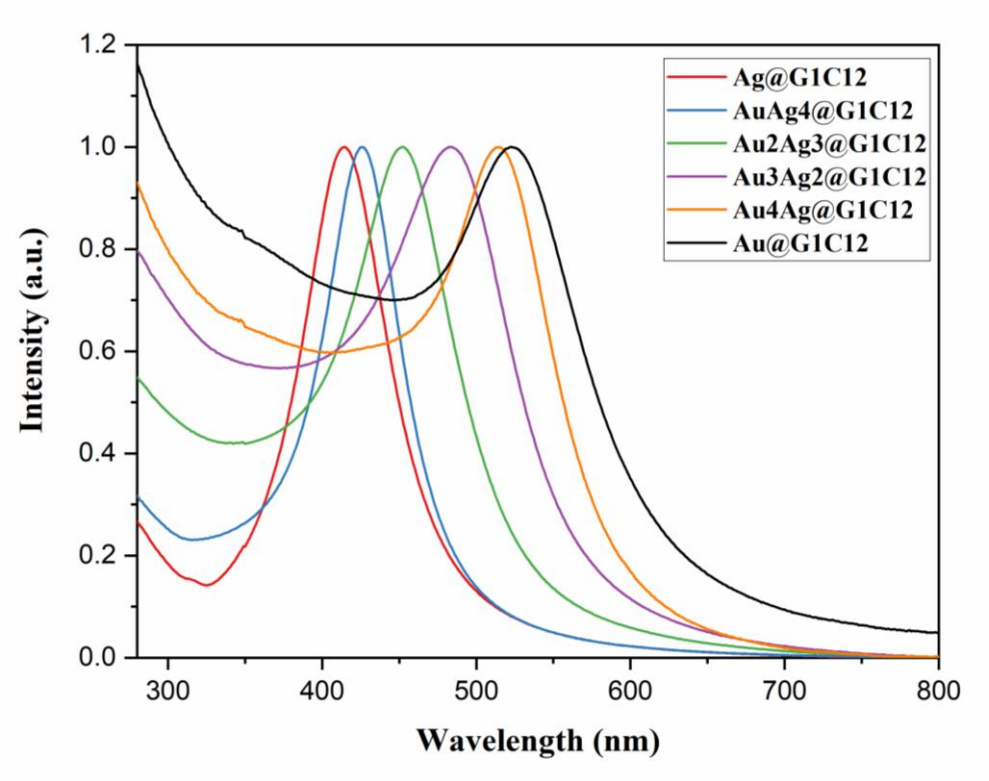

Appendix 16. ^{1}H NMR spectra of pure ligands (a) Olam (b) DDT (c) Ligand **2**.

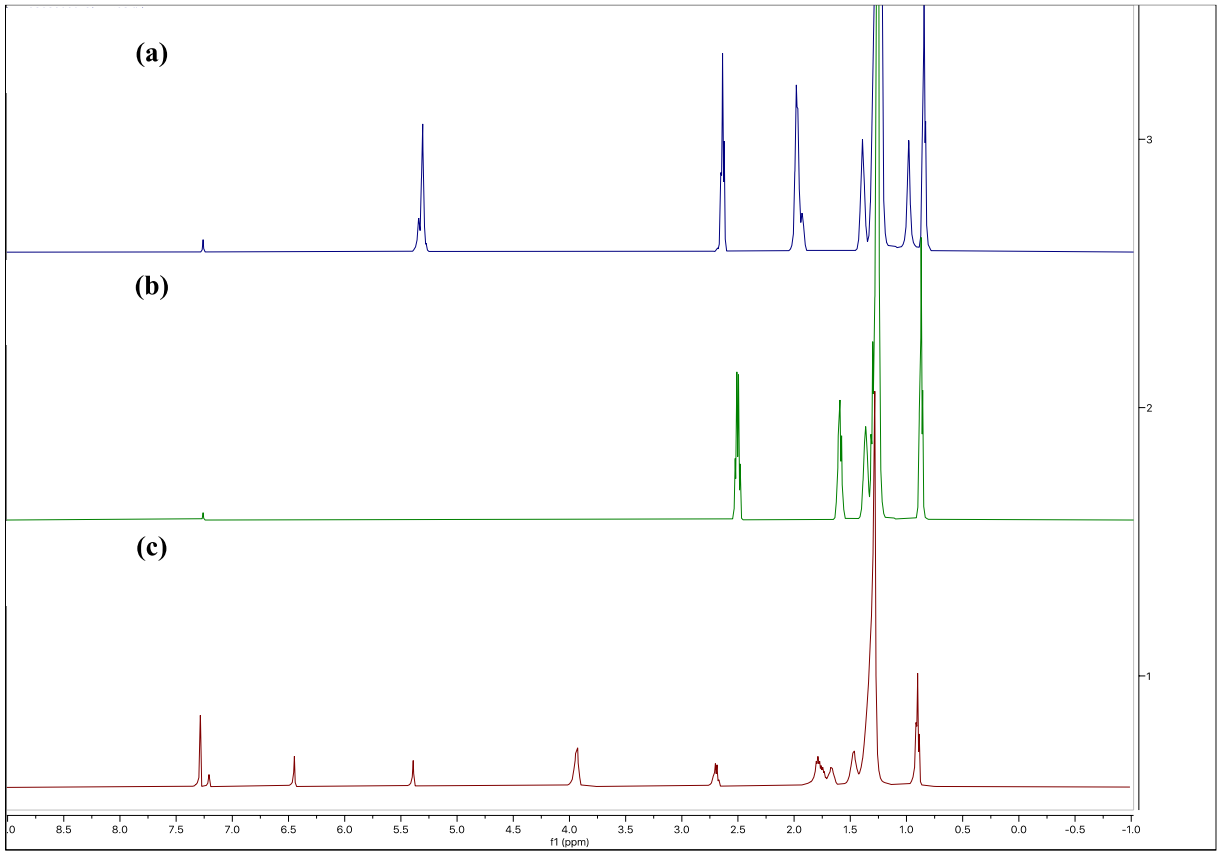

Appendix 17. ^{1}H NMR spectra of pure ligand **1**.

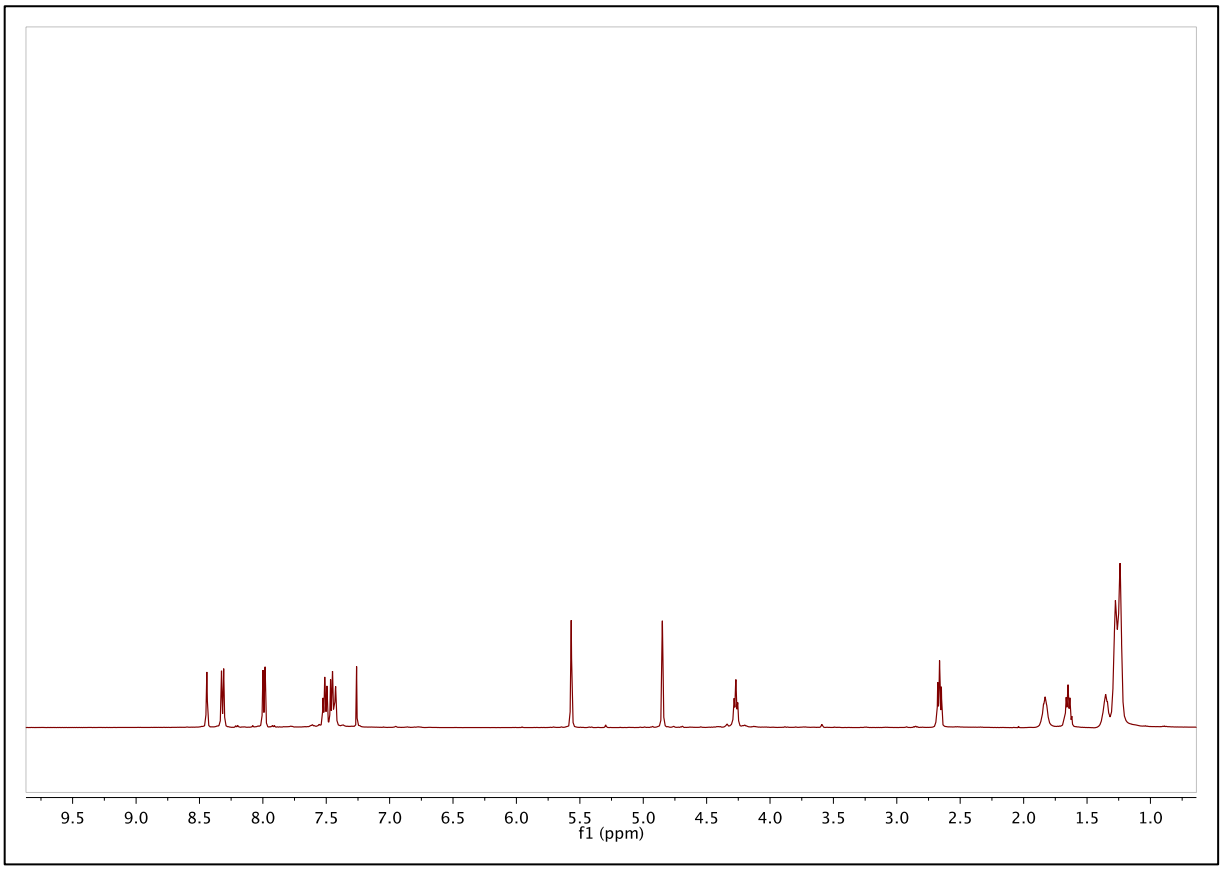

Appendix 18. ^{1}H NMR spectra of Au_xAg_{1-x}@Olam NPs (a) Ag, (b) $AuAg_4$, (c) Au_2Ag_3, (d) Au_3Ag_2, (e) Au_4Ag, (f) Au.

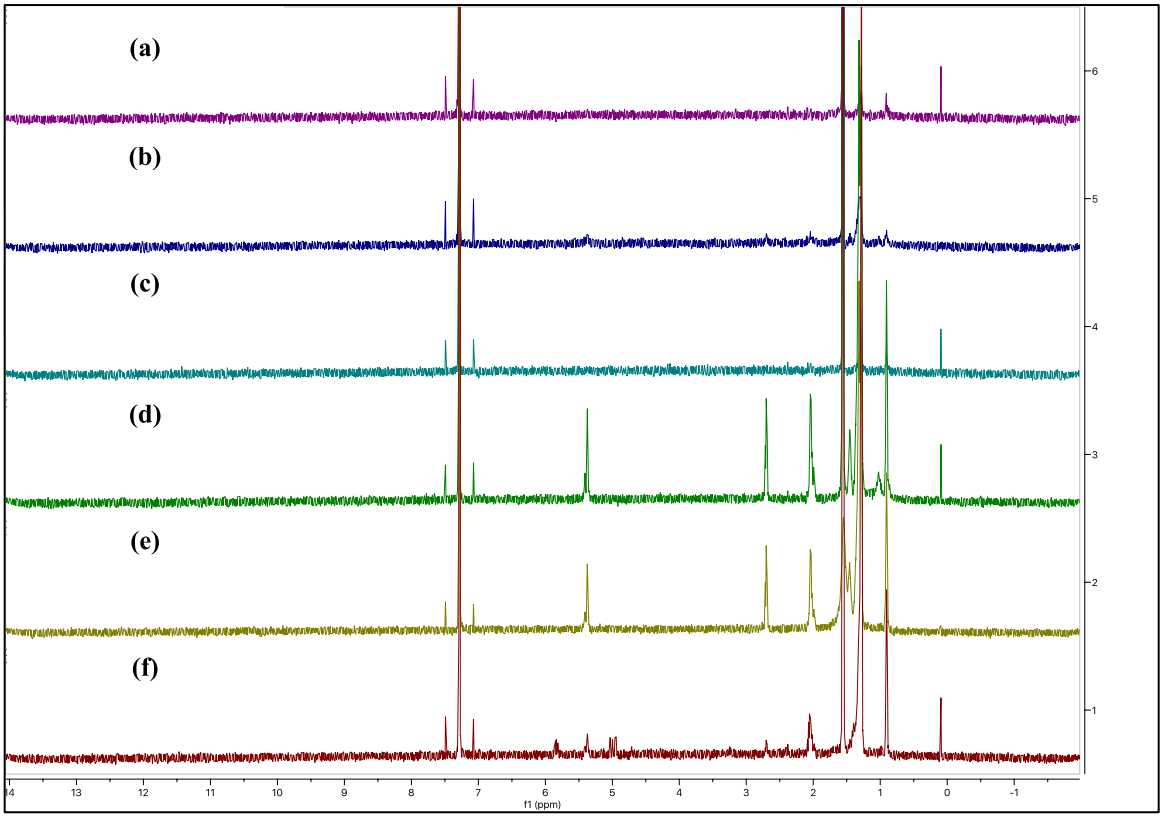

Appendix 19. ^{1}H NMR spectra of Au_xAg_{1-x}@DDT NPs (a) Ag, (b) $AuAg_4$, (c) Au_2Ag_3, (d) Au_3Ag_2, (e) Au_4Ag, (f) Au. No peak from Olam at 5.30 ppm is observable in all the samples, which indicates complete ligand exchange reactions.

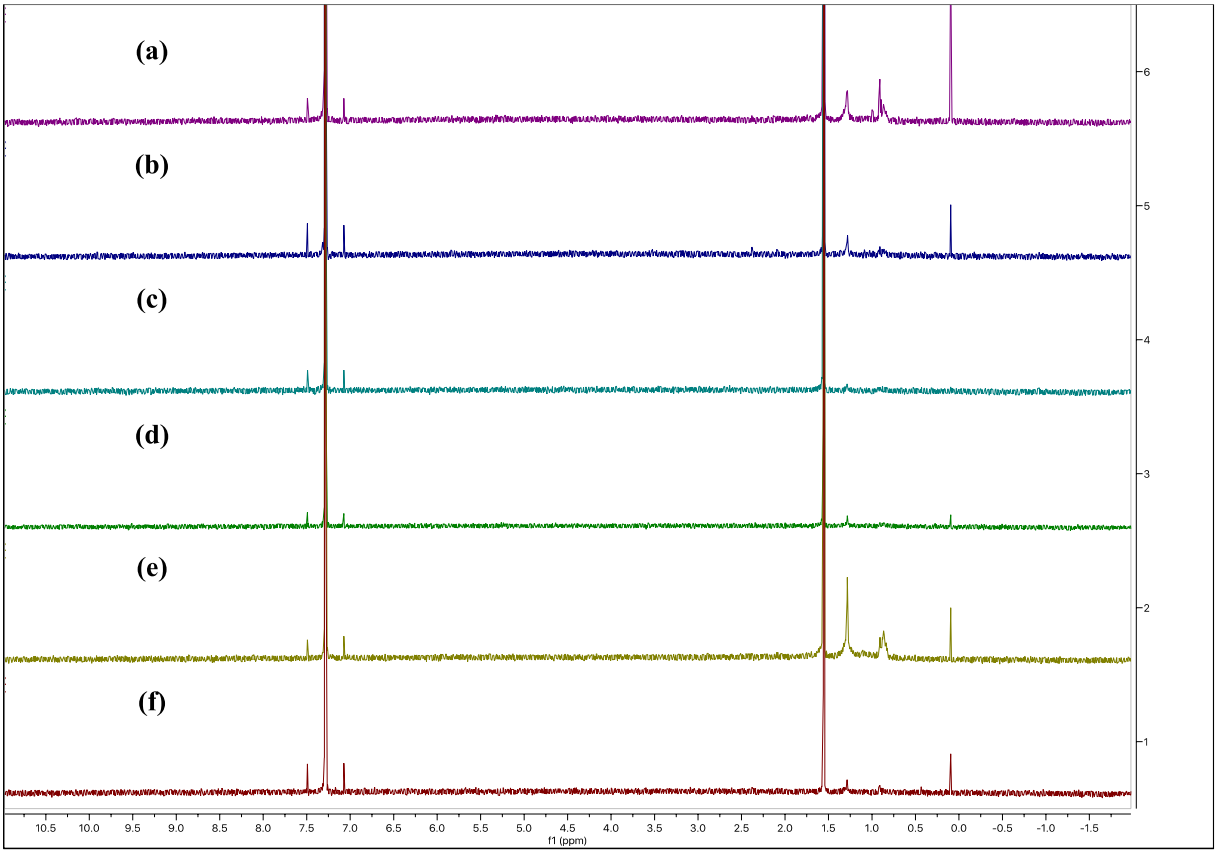

Appendix 20. ^{1}H NMR spectra of Au_xAg_{1-x}@**2** NPs (a) Ag, (b) $AuAg_4$, (c) Au_2Ag_3, (d) Au_3Ag_2, (e) Au_4Ag, (f) Au. Peak from Olam at 5.30 ppm is negligible in all the samples, indicating a complete exchange of the Olam with ligand **2**.